



CERN-EP-2019-150
 LHCb-PAPER-2018-049
 28 February 2020

Measurement of $\psi(2S)$ production cross-sections in proton-proton collisions at $\sqrt{s} = 7$ and 13 TeV

LHCb collaboration[†]

Abstract

The cross-sections of $\psi(2S)$ meson production in proton-proton collisions at $\sqrt{s} = 13$ TeV are measured with a data sample collected by the LHCb detector corresponding to an integrated luminosity of 275 pb^{-1} . The production cross-sections for prompt $\psi(2S)$ mesons and those for $\psi(2S)$ mesons from b -hadron decays ($\psi(2S)$ -from- b) are determined as functions of the transverse momentum, p_T , and the rapidity, y , of the $\psi(2S)$ meson in the kinematic range $2 < p_T < 20 \text{ GeV}/c$ and $2.0 < y < 4.5$. The production cross-sections integrated over this kinematic region are

$$\begin{aligned}\sigma(\text{prompt } \psi(2S), 13 \text{ TeV}) &= 1.430 \pm 0.005 \text{ (stat)} \pm 0.099 \text{ (syst) } \mu\text{b}, \\ \sigma(\psi(2S)\text{-from-}b, 13 \text{ TeV}) &= 0.426 \pm 0.002 \text{ (stat)} \pm 0.030 \text{ (syst) } \mu\text{b}.\end{aligned}$$

A new measurement of $\psi(2S)$ production cross-sections in pp collisions at $\sqrt{s} = 7$ TeV is also performed using data collected in 2011, corresponding to an integrated luminosity of 614 pb^{-1} . The integrated production cross-sections in the kinematic range $3.5 < p_T < 14 \text{ GeV}/c$ and $2.0 < y < 4.5$ are

$$\begin{aligned}\sigma(\text{prompt } \psi(2S), 7 \text{ TeV}) &= 0.471 \pm 0.001 \text{ (stat)} \pm 0.025 \text{ (syst) } \mu\text{b}, \\ \sigma(\psi(2S)\text{-from-}b, 7 \text{ TeV}) &= 0.126 \pm 0.001 \text{ (stat)} \pm 0.008 \text{ (syst) } \mu\text{b}.\end{aligned}$$

All results show reasonable agreement with theoretical calculations.

[†]Authors are listed at the end of this paper.

1 Introduction

The study of hadronic production of heavy quarkonia can provide important information about quantum chromodynamics (QCD). The production of heavy quark pairs, $Q\bar{Q}$, can be calculated with perturbative QCD, while the hadronisation of $Q\bar{Q}$ pairs into heavy quarkonia is nonperturbative and must be determined using input from experimental results. Heavy-quarkonium production therefore probes both perturbative and nonperturbative aspects of QCD by providing stringent tests of theoretical models. Knowledge of hadronic production of heavy quarkonium has been significantly improved in the past forty years [1, 2], but the mechanism behind it is still not fully understood. Colour-singlet model calculations [3–9] require that the intermediate $Q\bar{Q}$ state is colourless and has the same J^{PC} quantum numbers as those of the outgoing quarkonium state. In the nonrelativistic QCD (NRQCD) approach [10, 11], intermediate $Q\bar{Q}$ states with all possible colour-spin-parity quantum numbers have nonzero probability to be transformed into the desired quarkonium. The transition probability of a $Q\bar{Q}$ pair into the quarkonium state is described by a long-distance matrix element (LDME), which is assumed to be universal and can be determined from experimental data.

In high-energy proton-proton (pp) collisions, charmonium states can be produced directly from hard collisions of partons inside the protons, through the feed-down from excited states, or via weak decays of b hadrons. The first two contributions, which cannot be distinguished experimentally, are referred to as prompt production; while the third component can be separated from prompt production by exploiting the lifetime of b -hadrons. For prompt J/ψ production the feed-down contribution is large, mostly from radiative decays of χ_{cJ} ($J = 0, 1, 2$) mesons. This complicates the comparison between theoretical calculations and experimental results. On the contrary, the feed-down contribution to $\psi(2S)$ mesons is negligible [12], thus theoretical calculations can be directly compared with measurements.

The studies of heavy quarkonium production are crucial to separate the contributions of single parton scattering (SPS) [13] and double parton scattering (DPS) [14] to multiple-quarkonium production. Multiple-quarkonium production through the SPS process shares the same LDMEs as the single quarkonium production, thus providing a new method to test the theoretical calculations. The DPS process can reveal the transverse profile of partons inside the proton. Further theoretical and experimental works provide deeper insights on how to interpret the production mechanism of multiple quarkonia. In particular, additional data help in improving the precision of LDME determination.

The differential cross-sections of inclusive $\psi(2S)$ meson production in $p\bar{p}$ collisions at centre-of-mass energies of $\sqrt{s} = 1.8$ and 1.96 TeV were measured by the CDF experiment at the Fermilab Tevatron Collider [15, 16], and in pp collisions at $\sqrt{s} = 7$ TeV [17–22], 8 TeV [22], and 13 TeV [23] with LHC data. This paper presents measurements of $\psi(2S)$ production cross-sections in pp collisions using a data sample collected by LHCb in 2015 (2011) corresponding to an integrated luminosity of $275 \pm 11 \text{ pb}^{-1}$ at $\sqrt{s} = 13$ TeV ($614 \pm 11 \text{ pb}^{-1}$ at $\sqrt{s} = 7$ TeV). The $\psi(2S)$ mesons from prompt production are abbreviated as “prompt $\psi(2S)$ ”, while those from b -hadron decays are abbreviated as “ $\psi(2S)$ -from- b ”. The $\psi(2S)$ mesons are reconstructed through their decay mode $\psi(2S) \rightarrow \mu^+ \mu^-$. The double-differential production cross-sections of prompt $\psi(2S)$ and $\psi(2S)$ -from- b as functions of transverse momentum p_T and rapidity y and their integrated production cross-sections are measured, assuming zero polarisation of the $\psi(2S)$ meson. The kinematic

region of the measurement at 13 TeV (7 TeV) is $2 < p_T < 20 \text{ GeV}/c$ ($3.5 < p_T < 14 \text{ GeV}/c$) and $2.0 < y < 4.5$. Compared to the previous LHCb measurement at 7 TeV using 2010 data [18], the new analysis at 7 TeV has several advantages: the 2011 data sample is much larger than that in the previous measurement corresponding to an integrated luminosity of 36 pb^{-1} , the previous measurement did not provide the $\psi(2S)$ production cross-section as a function of the rapidity y because of the limited sample size, and the same final state and offline selection criteria as those in the 13 TeV measurement are used in the new 7 TeV measurement. This guarantees that the maximum number of systematic uncertainties cancel in the cross-section ratio between 13 TeV and 7 TeV, which is measured in the present analysis. This represents a more stringent test of the theoretical models, since many of the experimental and theoretical uncertainties cancel. Finally, the $\psi(2S)$ meson differential production cross-sections are compared with those of the J/ψ meson at $\sqrt{s} = 13 \text{ TeV}$ [24].

2 Detector and simulation

The LHCb detector [25, 26] is a single-arm forward spectrometer covering the pseudorapidity range $2 < \eta < 5$, designed for the study of particles containing b or c quarks. The detector includes a high-precision tracking system consisting of a silicon-strip vertex detector surrounding the pp interaction region [27], a large-area silicon-strip detector located upstream of a dipole magnet with a bending power of about 4 Tm, and three stations of silicon-strip detectors and straw drift tubes [28, 29] placed downstream of the magnet. The tracking system provides a measurement of the momentum, p , of charged particles with a relative uncertainty that varies from 0.5% at low momentum to 1.0% at $200 \text{ GeV}/c$. The minimum distance of a track to a primary vertex (PV), the impact parameter (IP), is measured with a resolution of $(15 + 29/p_T) \mu\text{m}$, where p_T is in GeV/c . Different types of charged hadrons are distinguished using information from two ring-imaging Cherenkov detectors [30]. Photons, electrons and hadrons are identified by a calorimeter system consisting of scintillating-pad (SPD) and preshower detectors, an electromagnetic calorimeter and a hadronic calorimeter. Muons are identified by a system composed of alternating layers of iron and multiwire proportional chambers [31]. The online event selection is performed by a trigger [32], which consists of a hardware stage, based on information from the calorimeter and muon systems, followed by a software stage, which applies a full event reconstruction.

Simulated samples are used to evaluate the $\psi(2S)$ detection efficiency. In the simulation, pp collisions are generated using PYTHIA 8 [33, 34] with a specific LHCb configuration [35]. Decays of unstable particles are described by EVTGEN [36], in which final-state radiation is generated using PHOTOS [37]. Both the leading-order colour-singlet and colour-octet contributions are included in the generated prompt charmonium states [35, 38]. These states are generated with zero polarisation. The interaction of the generated particles with the detector, and its response, are implemented using the GEANT4 toolkit [39] as described in Ref. [40].

3 Selection of $\psi(2S)$ candidates

The decay channel $\psi(2S) \rightarrow \mu^+ \mu^-$ is used in the measurements of the $\psi(2S)$ production cross-sections at both 13 TeV and 7 TeV. The same strategy is used for both analyses, except for different trigger requirements. The hardware trigger selects events that contain two tracks consistent with muon hypotheses, and the product of the transverse momenta of the two muons is required to be greater than $(1.3 \text{ GeV}/c)^2$. At the software trigger stage the two muons are required to be oppositely charged, to have good track quality, to form a good-quality vertex, and to each have a momentum larger than $6 \text{ GeV}/c$. The invariant mass of the $\psi(2S)$ candidates is required to be within the range $3566 < m_{\mu^+ \mu^-} < 3806 \text{ MeV}/c^2$. The transverse momentum of each muon is required to be larger than $0.3 \text{ GeV}/c$ ($0.5 \text{ GeV}/c$) and that of the $\psi(2S)$ candidate is required to be larger than $2 \text{ GeV}/c$ ($3.5 \text{ GeV}/c$) for the 13 TeV (7 TeV) data trigger. Due to the different triggers, the $\psi(2S)$ candidates are selected in different p_T ranges. For the 13 TeV data taking, an alignment and calibration of the detector is performed in near real-time [41] and updated constants are made available for the trigger.

To suppress the background associated to random combination of tracks (combinatorial) more stringent criteria are applied offline on the $\psi(2S)$ vertex fit quality, the muon kinematics and particle identification requirements. Each muon must have $p_T > 1.2 \text{ GeV}/c$ and $2.0 < \eta < 4.9$. At least one PV should be reconstructed in the event from at least four tracks in the vertex detector.

For events with more than one PV, the $\psi(2S)$ candidate is associated to the PV for which the difference in the χ^2 of the PV fit with and without the $\psi(2S)$ candidate is the smallest. This is equivalent to select the vertex with respect to which the signal candidate has the smallest impact parameter, compared to resolution. Simulation studies have shown that, using the above procedure, the fraction of candidates associated to the wrong PV is 0.3%, which is negligible. To select $\psi(2S)$ candidates, additional requirements on the pseudo decay time, t_z , $|t_z| < 10 \text{ ps}$, and its uncertainty, σ_{t_z} , $\sigma_{t_z} < 0.3 \text{ ps}$, are applied. The pseudo decay time t_z is defined as

$$t_z = \frac{(z_{\psi(2S)} - z_{\text{PV}}) \times M_{\psi(2S)}}{p_z}, \quad (1)$$

where $z_{\psi(2S)}$ (z_{PV}) is the z coordinate of the reconstructed $\psi(2S)$ decay vertex (the PV), p_z is the z -component of the measured $\psi(2S)$ momentum, and $M_{\psi(2S)}$ is the world average $\psi(2S)$ mass [12]. The z -axis is the direction of the proton beam pointing downstream into the LHCb acceptance [25]. The pseudo decay time defined above provides a good approximation of the b -hadron decay time [42] and is used to separate prompt $\psi(2S)$ and $\psi(2S)$ -from- b candidates.

4 Cross-section determination

The double-differential production cross-section for prompt $\psi(2S)$ or $\psi(2S)$ -from- b in a given (p_T, y) bin is defined as

$$\frac{d^2\sigma}{dy dp_T} = \frac{N(p_T, y)}{\varepsilon_{\text{tot}}(p_T, y) \times \mathcal{L}_{\text{int}} \times \mathcal{B} \times \Delta y \times \Delta p_T}, \quad (2)$$

where $N(p_T, y)$ is the signal yield, $\varepsilon_{\text{tot}}(p_T, y)$ is the total detection efficiency of the $\psi(2S) \rightarrow \mu^+ \mu^-$ decay evaluated independently for prompt $\psi(2S)$ or $\psi(2S)$ -from- b in the given (p_T, y) bin, \mathcal{L}_{int} is the integrated luminosity, \mathcal{B} is the branching fraction of the decay $\psi(2S) \rightarrow \mu^+ \mu^-$, and $\Delta p_T = 1 \text{ GeV}/c$ and $\Delta y = 0.5$ are the bin widths. The integrated luminosity is determined using the beam-gas imaging and, for the 7 TeV data, also the van der Meer scan methods [43]. Assuming lepton universality in electromagnetic decays, $\mathcal{B}(\psi(2S) \rightarrow e^+ e^-) = (7.89 \pm 0.17) \times 10^{-3}$ [44] is used in Eq. 2, taking advantage of the much smaller uncertainty compared to the $\psi(2S) \rightarrow \mu^+ \mu^-$ decay. The difference of the two branching fractions introduced by the mass difference between electrons and muons is negligible.

The yields of prompt $\psi(2S)$ and $\psi(2S)$ -from- b candidates in each (p_T, y) bin are determined from a two-dimensional extended unbinned maximum-likelihood fit to the distributions of the invariant mass, $m_{\mu^+ \mu^-}$, and t_z of the $\psi(2S)$ candidates. The correlation between $m_{\mu^+ \mu^-}$ and t_z is found to be negligible. The invariant-mass distribution of the signal candidates in each bin is described by the sum of two Crystal Ball (CB) functions [45] with a common mean value and different widths. The parameters of the power-law tails, the relative fractions and the difference between the widths of the two CB functions are fixed to values obtained from simulation, leaving the mean value and the width of one of the CB functions as free parameters. The invariant-mass distribution of the combinatorial background is described by an exponential function with the slope parameter free to vary in the fit. The t_z distribution of prompt $\psi(2S)$ mesons is described by a Dirac δ function at $t_z = 0$, and that of $\psi(2S)$ -from- b by an exponential function, both convolved with the sum of two Gaussian functions. A $\psi(2S)$ candidate can also be associated to a wrong PV, resulting in a long tail component in the t_z distribution. This shape is modelled from data by calculating t_z between the $\psi(2S)$ candidate from a given event and the closest PV in the next event of the sample. The background t_z distribution is parametrised with an empirical function based on the observed shape of the t_z distribution in the $\psi(2S)$ mass sidebands ($3566 < m_{\mu^+ \mu^-} < 3620 \text{ MeV}/c^2$ and $3750 < m_{\mu^+ \mu^-} < 3806 \text{ MeV}/c^2$). It is parametrised as the combination of a Dirac δ function and the sum of five exponential functions, three for positive t_z and two for negative t_z . This sum is convolved with the sum of two Gaussian functions. All parameters of the background t_z distribution are fixed to values determined from the $\psi(2S)$ mass sidebands independently in each (p_T, y) bin. Figure 1 shows as an example the $m_{\mu^+ \mu^-}$ and t_z distributions in the kinematic bin corresponding to $5 < p_T < 6 \text{ GeV}/c$ and $2.5 < y < 3.0$ for the 13 TeV data sample. The one-dimensional projections of the fit result are also presented. The total signal yields of prompt $\psi(2S)$ and $\psi(2S)$ -from- b in the kinematic range for the 13 TeV sample are $(440.7 \pm 1.2) \times 10^3$ and $(140.0 \pm 0.5) \times 10^3$, and for the 7 TeV sample are $(433.9 \pm 0.9) \times 10^3$ and $(115.1 \pm 0.4) \times 10^3$, respectively.

The total efficiency, ε_{tot} , in each kinematic bin is determined as the product of the geometrical acceptance of the detector and the efficiencies of particle reconstruction, event selection, muon identification and trigger requirements. The detector acceptance, selection and trigger efficiencies are calculated using simulated samples in each (p_T, y) bin, independently for prompt $\psi(2S)$ and $\psi(2S)$ -from- b . The trigger efficiencies are also validated using data, as explained in Section 5. The track reconstruction and the muon-identification efficiencies are evaluated using simulated samples and calibrated with data. The efficiencies of prompt $\psi(2S)$ and those of $\psi(2S)$ -from- b are very similar.

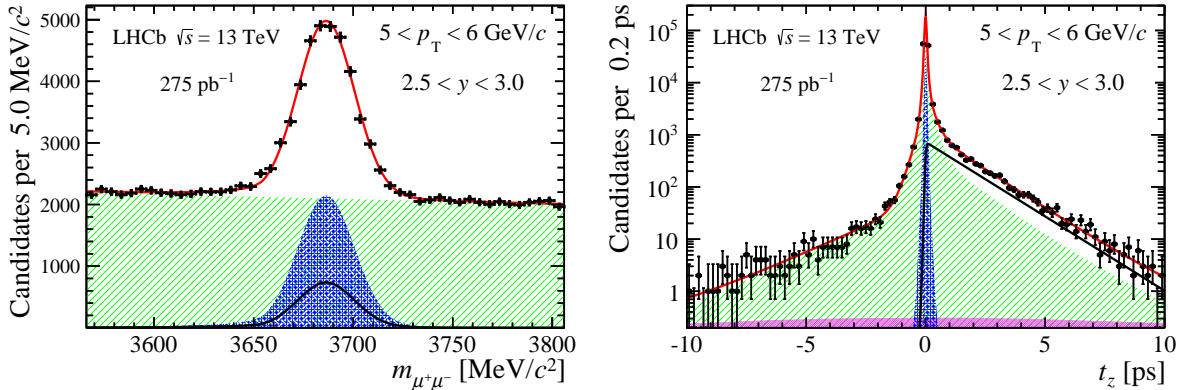


Figure 1: Distributions of (left) the invariant mass $m_{\mu^+\mu^-}$ and (right) pseudo decay time t_z of selected $\psi(2S)$ candidates in the kinematic bin of $5 < p_T < 6 \text{ GeV}/c$ and $2.5 < y < 3.0$ in the 13 TeV data sample. Projections of the two-dimensional fit result are also shown. The solid (red) line is the total fit function, the shaded (green) area corresponds to the background component. The prompt $\psi(2S)$ contribution is shown in cross-hatched (blue) area, $\psi(2S)$ -from- b in a solid (black) line and the tail contribution due to the association of $\psi(2S)$ with the wrong PV is shown in filled (magenta) area. The tail contribution is invisible in the invariant-mass plot.

5 Systematic uncertainties

A variety of sources of systematic uncertainty are studied as described below and are summarised in Table 1. For the uncertainties that vary in kinematic bins, the largest uncertainties always appear in the bins with small sample sizes.

The uncertainty related to the modelling of the signal mass shape is studied by replacing the baseline model with a kernel-density estimated distribution [46] obtained from the simulated sample in each kinematic bin. In order to account for the resolution difference between data and simulation, a Gaussian function is used to smear the shape of the

Table 1: Systematic uncertainties on the $\psi(2S)$ cross-section measurements. The uncertainty from the t_z fit only affects the $\psi(2S)$ -from- b result. Uncertainties labelled with “*” are correlated between kinematic bins.

Source	13 TeV (%)	7 TeV (%)
Signal mass shape*	0.0–4.1	0.0–8.5
Radiative tail*	1.0	1.0
Tracking*	(0.1–2.4) \oplus (2 \times 0.8)	(0.7–3.0) \oplus (2 \times 0.4)
Muon ID*	(0.1–1.1) \oplus (0.1–4.6)	(0.7–8.9) \oplus (0.4–5.4)
Trigger*	0.1–9.3	0.0–4.4
Kinematic spectrum	0.0–2.0	0.0–4.9
Luminosity*	3.9	1.7
$\mathcal{B}(\psi(2S) \rightarrow e^+e^-)^*$	2.2	2.2
Simulated sample size (prompt $\psi(2S)$)	0.7–11.5	1.3–13.1
Simulated sample size ($\psi(2S)$ -from- b)	0.8–5.7	1.2–9.5
t_z fit* ($\psi(2S)$ -from- b only)	0.1–8.4	0.1–9.2

distribution in simulation. The relative difference of the signal yield in each kinematic bin, 0.0–4.1% (0.0–8.5%) for the 13 TeV (7 TeV) sample, is taken as the systematic uncertainty due to signal mass shape.

Due to the presence of final-state radiation in the $\psi(2S) \rightarrow \mu^+ \mu^-$ decay, a fraction of $\psi(2S)$ candidates fall outside the mass window used to determine the signal yields. The efficiency of the selection of the mass window is estimated using simulated samples, and the imperfect modelling of the radiation is studied by comparisons of the radiative tails between simulation and data, from which an uncertainty of 1.0% is assigned to the cross-sections in all kinematic bins.

The track detection efficiencies are determined from a simulated sample in each (p_T, y) bin of the $\psi(2S)$ meson, and are corrected by using $J/\psi \rightarrow \mu^+ \mu^-$ decays reconstructed in a control data sample and in simulation. These efficiencies are calculated as functions of p and η with a tag-and-probe approach [47]. The uncertainties due to the finite size of the control samples are propagated to the results using a large number of pseudoexperiments. In each pseudoexperiment, a new efficiency-correction ratio in each (p_T, y) bin is generated according to a Gaussian distribution where the original ratio and its uncertainty are used as the Gaussian mean and standard deviation, respectively. The contribution to the systematic uncertainty in each kinematic bin of $\psi(2S)$ mesons varies from 0.1% (0.7%) to 2.4% (3.0%) for the 13 TeV (7 TeV) data sample. The distribution of the number of SPD hits in simulation is weighted to match that in data to correct the effect of the detector occupancy. As a crosscheck the number of tracks is used as an alternative weighting variable. The tracking efficiencies are found to be different when different variables are used. Therefore, an additional systematic uncertainty of 0.8% (0.4%) per muon track is assigned for the 13 TeV (7 TeV) sample.

The muon identification efficiency is determined from simulation and calibrated with a data sample of $J/\psi \rightarrow \mu^+ \mu^-$ decays. The statistical uncertainty due to the finite size of the calibration sample is propagated to the final results using pseudoexperiments. The resulting uncertainties vary from 0.1% (0.7%) to 1.1% (8.9%) in different (p_T, y) bins for the 13 TeV (7 TeV) sample. The uncertainty related to the kinematic binning scheme of the calibration samples is studied by changing the size and the boundaries of the p and η bins, and number of SPD hits. This leads to systematic uncertainties of 0.1–4.6% (0.4–5.4%) for the 13 TeV (7 TeV) sample.

The trigger efficiency is determined from simulated samples. To estimate the systematic uncertainty, a tag-and-probe method is used to estimate the trigger efficiencies in each (p_T, y) bin of a $\psi(2S)$ data sample that is independent of the detection of $\psi(2S)$ signals [32]. The same procedure is applied to the simulated $\psi(2S)$ samples, and the relative difference of efficiencies between data and simulation in each kinematic bin, 0.1–9.3% (0.0–4.4%) for the 13 TeV (7 TeV) sample, is taken as a systematic uncertainty.

The p_T and y distributions of $\psi(2S)$ mesons in simulation and in data could be different within each kinematic bin due to the finite bin size, causing differences in efficiencies. The possible discrepancy is studied by weighting the kinematic distribution in simulation to match that in data. All efficiencies are recalculated, and the relative differences of the total efficiencies between the new and the nominal results, which are found to be in the range 0.0–2.0% (0.0–4.9%) for the 13 TeV (7 TeV) sample, are taken as systematic uncertainties.

The integrated luminosity is determined using the beam-gas imaging method for the 13 TeV data sample, and by a combination of the beam-gas imaging and van der

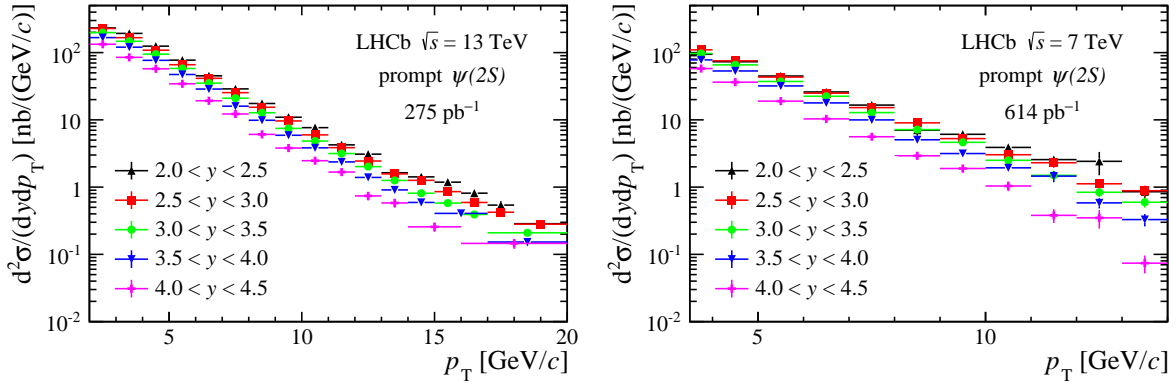


Figure 2: Double-differential production cross-sections of prompt $\psi(2S)$ as functions of p_T in bins of y at (left) 13 TeV and (right) 7 TeV. The statistical and systematic uncertainties are added in quadrature. The $\psi(2S)$ meson is assumed to be produced unpolarised.

Meer scan methods [43] for the 7 TeV data sample. The uncertainty associated with the luminosity determination is 3.9% (1.7%) for the 13 TeV (7 TeV) sample. The uncertainty of the branching fraction of the $\psi(2S) \rightarrow e^+e^-$ decay, 2.2%, is taken as a systematic uncertainty [44]. The limited size of the simulated sample in each bin leads to uncertainties of 0.7–11.5% (1.3–13.1%) for prompt $\psi(2S)$ and 0.8–5.7% (1.2–9.5%) for $\psi(2S)$ -from- b for the 13 TeV (7 TeV) sample, and are smaller than or comparable with the data statistical uncertainty in each bin.

There are sources of systematic uncertainties that are related to the t_z variable, the effects of which are notable for $\psi(2S)$ -from- b and are negligible for prompt $\psi(2S)$. The modelling of the t_z resolution is modified by adding a third Gaussian to the nominal resolution model. The variation in the $\psi(2S)$ -from- b fraction F_b is found to be negligible. An alternative method is adopted to estimate the systematic uncertainty due to the modelling of the background t_z distribution. In this method, the background distribution is obtained with the *sPlot* technique [48] using the invariant mass as the discriminating variable. The t_z distribution is then parametrised for the two-dimensional fits to obtain the fraction F_b . The relative difference of F_b in each kinematic bin between the two methods is taken as a systematic uncertainty. The total systematic uncertainty on the $\psi(2S)$ -from- b cross-section related to the t_z fit model is 0.1–8.4% (0.1–9.2%) for the 13 TeV (7 TeV) sample.

6 Results

6.1 Production cross-sections

The double-differential production cross-sections for prompt $\psi(2S)$ and $\psi(2S)$ -from- b are measured as functions of p_T and y assuming no polarisation of $\psi(2S)$ mesons. The results are shown in Figs. 2 and 3, respectively. The corresponding values are listed in Tables 2, 3, 4, and 5 in Appendix A.

By integrating the double-differential results over y in the range $2.0 < y < 4.5$, the differential production cross-sections of prompt $\psi(2S)$ and $\psi(2S)$ -from- b as functions of p_T are shown in Fig. 4. The results of prompt $\psi(2S)$ production are compared

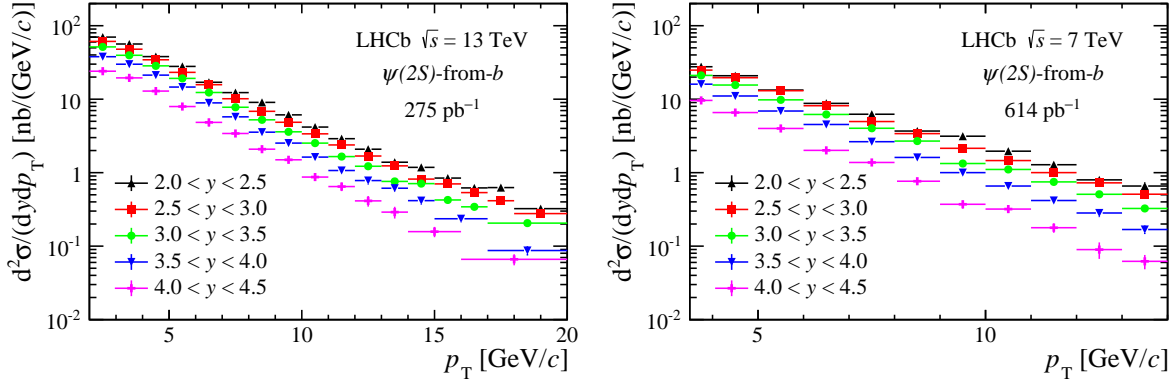


Figure 3: Double-differential production cross-sections of $\psi(2S)$ -from- b as functions of p_T in bins of y at (left) 13 TeV and (right) 7 TeV. The statistical and systematic uncertainties are added in quadrature. The $\psi(2S)$ meson is assumed to be produced unpolarised.

with the theoretical calculations based on NRQCD [49], and those of $\psi(2S)$ -from- b are compared with the fixed-order-plus-next-leading-logarithm (FONLL) calculations [50]. The differential cross-section as function of y at 13 TeV (7 TeV) is obtained by integrating the double-differential results over p_T in the range $2 < p_T < 20 \text{ GeV}/c$ ($3.5 < p_T < 14 \text{ GeV}/c$). The results are presented in Fig. 5. The theoretical calculations based on FONLL are shown for $\psi(2S)$ -from- b . The NRQCD calculations are omitted since they are not reliable in the low p_T region [51]. The values of the differential cross-sections are shown in Tables 6, 7, 8, and 9 in Appendix A. In the NRQCD calculations, only the dominant uncertainties associated with the LDMEs are considered [49]. The FONLL calculations include the uncertainty due to b -quark mass and the scales of renormalisation and factorisation. The NRQCD calculations show reasonable agreement with experimental data for $p_T > 7 \text{ GeV}/c$. The FONLL calculations agree well with the measurements. The production cross-sections of prompt $\psi(2S)$ and $\psi(2S)$ -from- b integrated in the kinematic range $2.0 < y < 4.5$ and $2 < p_T < 20 \text{ GeV}/c$ at 13 TeV, are measured to be:

$$\begin{aligned}\sigma(\text{prompt } \psi(2S), 13 \text{ TeV}) &= 1.430 \pm 0.005 \text{ (stat)} \pm 0.099 \text{ (syst) } \mu\text{b}, \\ \sigma(\psi(2S)\text{-from-}b, 13 \text{ TeV}) &= 0.426 \pm 0.002 \text{ (stat)} \pm 0.030 \text{ (syst) } \mu\text{b}.\end{aligned}$$

The production cross-sections of prompt $\psi(2S)$ and $\psi(2S)$ -from- b integrated in the kinematic range $2.0 < y < 4.5$ and $3.5 < p_T < 14 \text{ GeV}/c$ at 7 TeV, are measured to be:

$$\begin{aligned}\sigma(\text{prompt } \psi(2S), 7 \text{ TeV}) &= 0.471 \pm 0.001 \text{ (stat)} \pm 0.025 \text{ (syst) } \mu\text{b}, \\ \sigma(\psi(2S)\text{-from-}b, 7 \text{ TeV}) &= 0.126 \pm 0.001 \text{ (stat)} \pm 0.008 \text{ (syst) } \mu\text{b}.\end{aligned}$$

As mentioned above, these results are obtained under the assumption of zero polarisation of $\psi(2S)$ mesons. Possible polarisation of $\psi(2S)$ meson would affect the detection efficiency. This effect is studied for extreme cases of fully transverse and fully longitudinal polarisation corresponding to the parameter α be equal to +1 or -1, respectively, within the helicity frame [52] approach. Also the polarisation case of $\alpha = -0.2$, corresponding to a conservative limit of the $\psi(2S)$ polarisation measured at 7 TeV [53], is considered. Resulting scaling factors for prompt $\psi(2S)$ production cross-sections are listed in Appendix B in Tables 16, 17 and 18 for 13 TeV results, and in Tables 19, 20 and 21 for 7 TeV results, respectively.

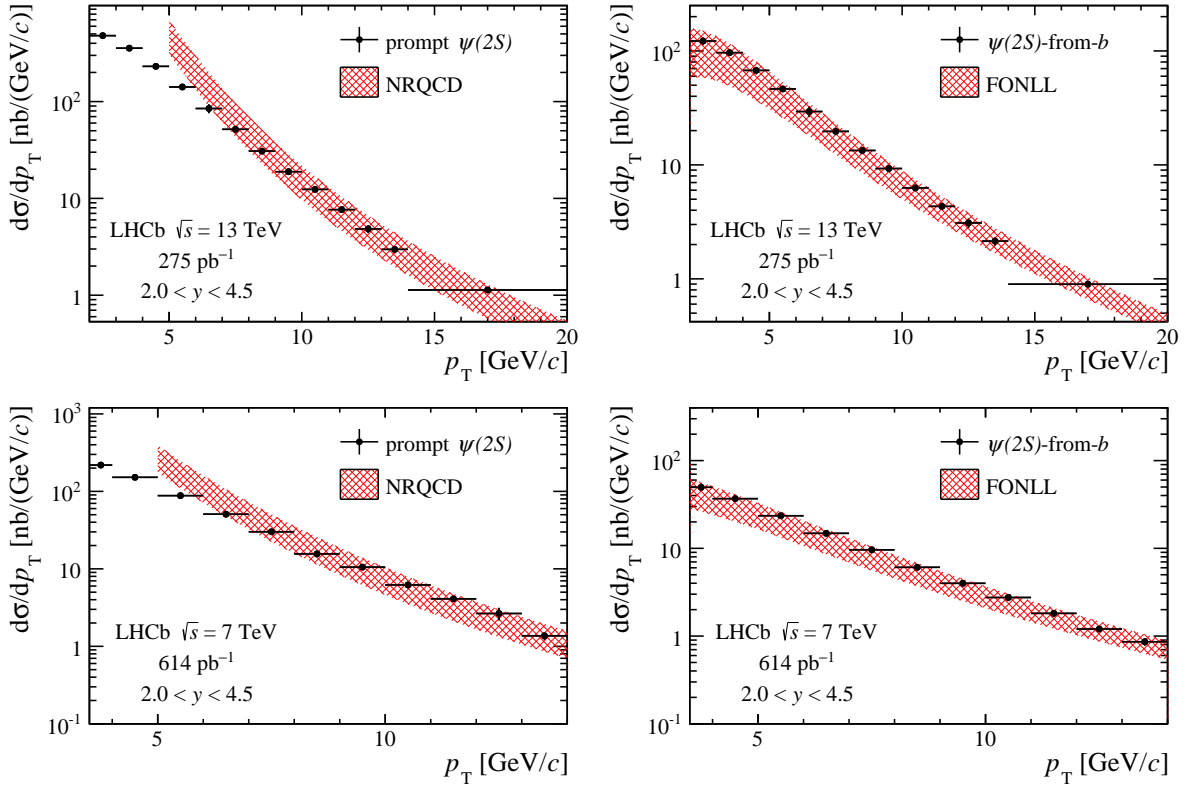


Figure 4: Differential production cross-sections as functions of p_T in the range $2.0 < y < 4.5$ for the (top) 13 TeV and (bottom) 7 TeV samples. The left-hand figures are for prompt $\psi(2S)$ and the results are compared with the NRQCD calculations [49]; the right-hand figures are for $\psi(2S)$ -from- b and the results are compared with the FONLL calculations [50].

6.2 Fraction of $\psi(2S)$ -from- b mesons

The fraction of $\psi(2S)$ -from- b is $F_b \equiv N_b/(N_b + N_p)$, where N_p is the efficiency-corrected signal yield of prompt $\psi(2S)$ and N_b is that of $\psi(2S)$ -from- b . The fractions F_b as functions of p_T and y are shown in Fig. 6. The corresponding values are presented in Table 10 in Appendix A. Only statistical uncertainties are shown owing to the cancellation of most systematic contributions, except for that due to the t_z fit, which is negligible. For each y bin, the fraction increases with increasing p_T of the $\psi(2S)$ mesons. For each p_T bin, the fraction decreases with increasing y of the $\psi(2S)$ mesons.

6.3 Comparison with J/ψ results at 13 TeV

The production cross-sections of $\psi(2S)$ mesons at 13 TeV are compared with those of J/ψ mesons measured by LHCb at $\sqrt{s} = 13$ TeV in the range $0 < p_T < 14$ GeV/ c and $2.0 < y < 4.5$ [24], where the J/ψ meson is also assumed to be produced with zero polarisation. The ratio, $R_{\psi(2S)/J/\psi}$, of the differential production cross-sections in the common range between prompt $\psi(2S)$ and prompt J/ψ mesons is shown in Fig. 7 as a function of p_T (y) integrated over $2.0 < y < 4.5$ ($2 < p_T < 14$ GeV/ c). The NRQCD calculation of $R_{\psi(2S)/J/\psi}$ for prompt productions [49] is also shown. The ratio of production cross-sections between $\psi(2S)$ -from- b and J/ψ -from- b is shown in Fig. 8 as a function of

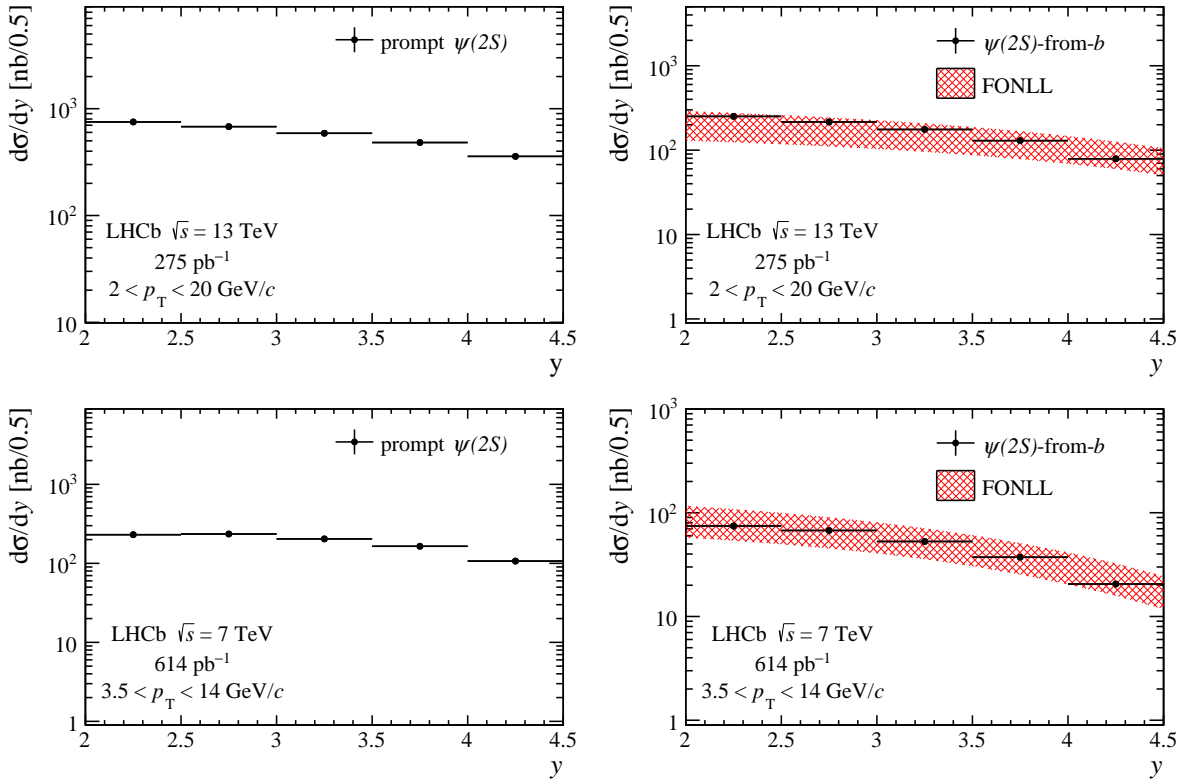


Figure 5: Differential production cross-sections as functions of y in the range $2 < p_T < 20 \text{ GeV}/c$ for the 13 TeV sample (top) and in the range $3.5 < p_T < 14 \text{ GeV}/c$ for the 7 TeV sample (bottom). The left figures are for prompt $\psi(2S)$, the right figures are for $\psi(2S)$ -from- b compared with the FONLL calculations [50].

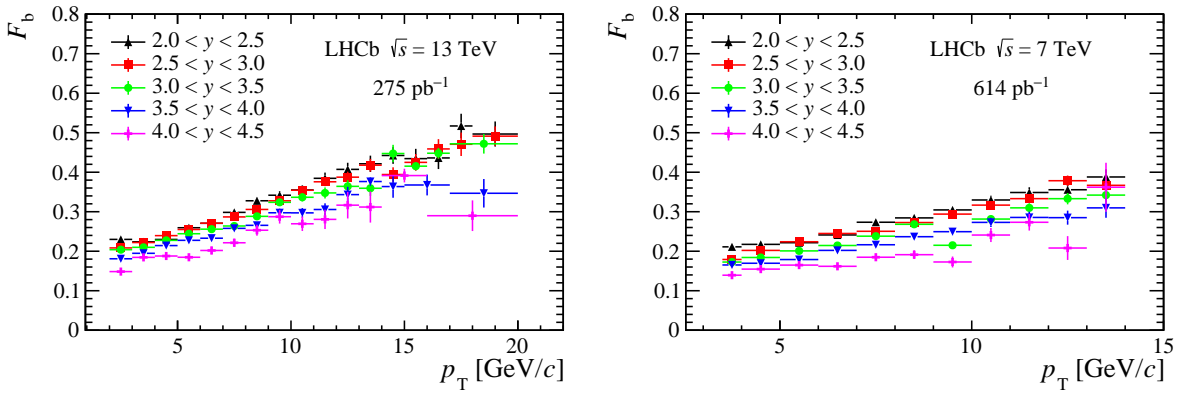


Figure 6: Fractions of $\psi(2S)$ -from- b in bins of p_T and y for the (left) 13 TeV and (right) 7 TeV samples. The error bars represent the statistical uncertainties.

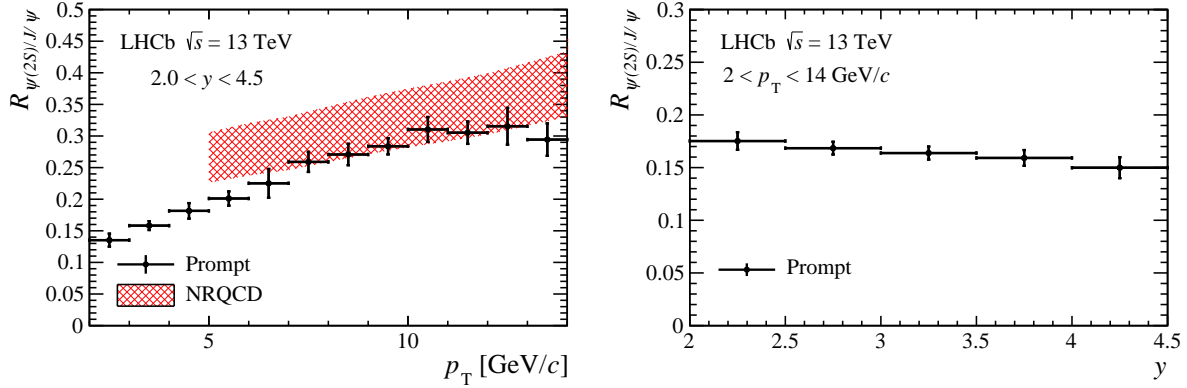


Figure 7: Ratios of differential cross-sections between prompt $\psi(2S)$ and prompt J/ψ mesons at 13 TeV as functions of (left) p_T and (right) y . The NRQCD predicted ratio [49] is shown in the left panel for comparison.

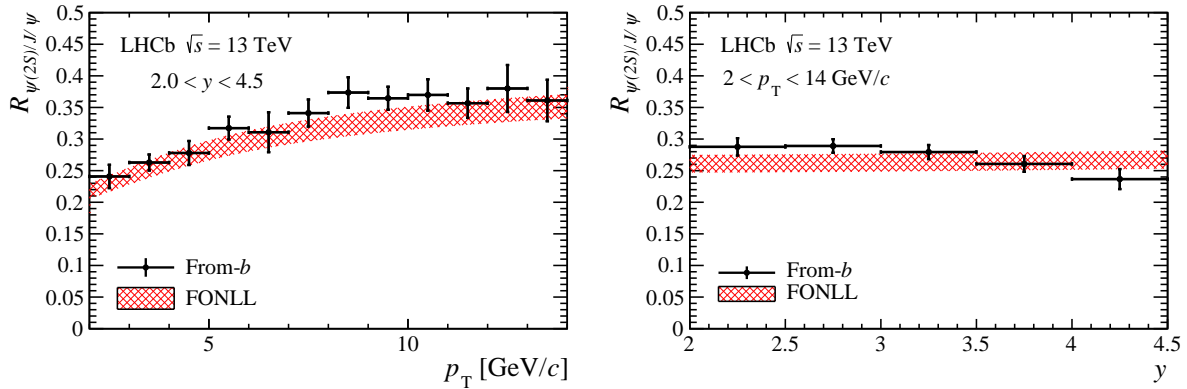


Figure 8: Ratios of differential cross-sections between $\psi(2S)$ -from- b and J/ψ mesons from b -hadron decays at 13 TeV as functions of (left) p_T and (right) y . The FONLL calculations [54] are shown for comparison.

p_T (y) integrated over $2.0 < y < 4.5$ ($2 < p_T < 14 \text{ GeV}/c$). The FONLL calculations [54] are compared to the measured values. To calculate these ratios from the measured cross-sections of $\psi(2S)$ and J/ψ mesons, the systematic uncertainties due to the luminosity, the tracking correction, and the fit model are considered to be fully correlated. All other uncertainties are assumed to be uncorrelated. The numerical results of the measured ratios are listed in Tables 12 and 13 in Appendix A. The FONLL prediction agrees well with the experimental data for the production cross-section ratio between $\psi(2S)$ -from- b and J/ψ mesons from b -hadron decays, while the NRQCD predictions show reasonable agreement with the measurements for prompt $\psi(2S)$ and prompt J/ψ .

6.4 Comparison between 13 TeV and 7 TeV

The production cross-sections of $\psi(2S)$ mesons in pp collisions at 13 TeV and 7 TeV are compared by means of their ratio, $R_{13/7}$. Figures 9 and 10 show the ratios as functions of p_T integrated over $2.0 < y < 4.5$ and as functions of y integrated over $3.5 < p_T < 14 \text{ GeV}/c$ for prompt $\psi(2S)$ and $\psi(2S)$ -from- b . The NRQCD (FONLL) calculations of $R_{13/7}$ for

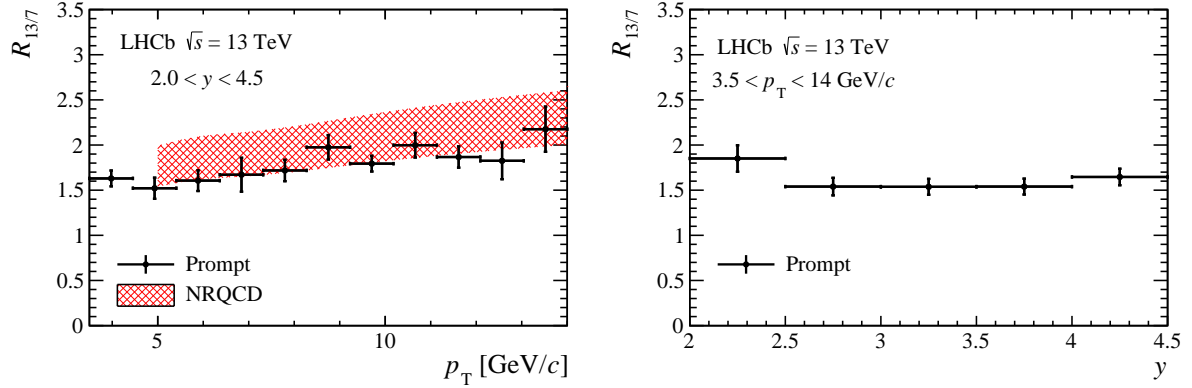


Figure 9: Ratio of differential production cross-sections between the 13 TeV and 7 TeV measurements as a function of (left) p_T integrated over y and (right) y integrated over p_T for prompt $\psi(2S)$ production. Theoretical calculations of NRQCD [49] are compared to the data on the left side.

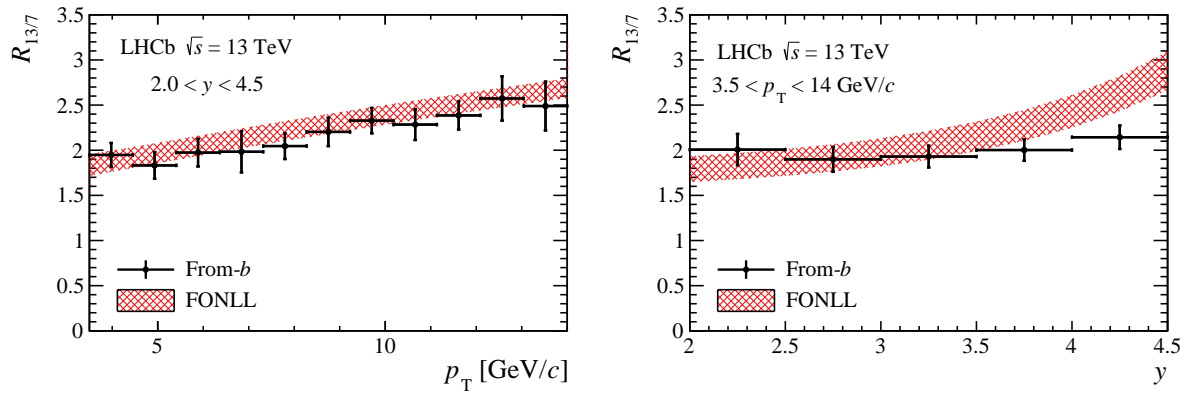


Figure 10: Ratio of differential production cross-sections between the 13 TeV and the 7 TeV measurements as a function of (left) p_T integrated over y and (right) y integrated over p_T for $\psi(2S)$ -from- b . Theoretical FONLL calculations [54] are compared to the data.

prompt $\psi(2S)$ ($\psi(2S)$ -from- b) are also shown in the left (right) panel for comparison. Both FONLL and NRQCD predictions on $R_{13/7}$ agree well with the corresponding experimental data. The measured ratios are also presented in Tables 14 and 15 in Appendix A.

For both the theoretical calculations and the experimental measurements, some of the uncertainties in the ratio cancel, which allows for a more precise comparison to theory. In the calculation of these ratios from the measured $\psi(2S)$ production cross-sections at 13 TeV and 7 TeV the systematic uncertainty related to the branching fraction is cancelled. The uncertainties due to the luminosity, the fit model and the tracking correction are partially correlated. Other uncertainties are assumed to be uncorrelated.

6.5 Measurement of the inclusive $b \rightarrow \psi(2S)X$ branching fraction

The reported results of the cross-section $\sigma(\psi(2S)\text{-from-}b, 13 \text{ TeV})$, in combination with the previous results about J/ψ production [24], can be used to determine the inclusive

branching fraction $\mathcal{B}(b \rightarrow \psi(2S)X)$. To achieve this, both results must be extrapolated to the full phase space, as they are measured only for a limited range of phase space. The extrapolation factors $\alpha_{4\pi}(\psi(2S))$ and $\alpha_{4\pi}(J/\psi)$ are determined with LHCb-tuned versions of Pythia 8 [33] for the $\psi(2S)$ and of Pythia 6 [34] for the J/ψ . The factors $\alpha_{4\pi}(\psi(2S))$ and $\alpha_{4\pi}(J/\psi)$ are found to be 7.29 and 5.20, respectively. In the ratio of the two factors,

$$\xi \equiv \frac{\alpha_{4\pi}(\psi(2S))}{\alpha_{4\pi}(J/\psi)} = 1.402,$$

most of the theoretical uncertainties are expected to cancel. Alternatively, the correction factor ξ can be obtained using FONLL calculations which uses different parton distribution functions. The values of ξ obtained from the two methods differ by 2.89 %.

With the definition of the ratio ξ , the $\mathcal{B}(b \rightarrow \psi(2S)X)$ branching fraction can be obtained from the ratio

$$\frac{\mathcal{B}(b \rightarrow \psi(2S)X)}{\mathcal{B}(b \rightarrow J/\psi X)} = \xi \frac{\sigma(\psi(2S)\text{-from-}b, 13 \text{ TeV})}{\sigma(J/\psi\text{-from-}b, 13 \text{ TeV})}. \quad (3)$$

By inserting the value $\sigma(J/\psi\text{-from-}b, 13 \text{ TeV}) = 2.25 \pm 0.01(\text{stat}) \pm 0.14(\text{syst}) \mu\text{b}$ [24] and the value of ξ , the ratio of the branching fractions is

$$\frac{\mathcal{B}(b \rightarrow \psi(2S)X)}{\mathcal{B}(b \rightarrow J/\psi X)} = 0.265 \pm 0.002(\text{stat}) \pm 0.015(\text{syst}) \pm 0.006(\mathcal{B}),$$

where possible correlations between uncertainties originating from $\psi(2S)\text{-from-}b$ and $J/\psi\text{-from-}b$, respectively, are taken into account. The last uncertainty is from the uncertainty of the branching fractions $\mathcal{B}(\psi(2S) \rightarrow e^+e^-)$ and $\mathcal{B}(J/\psi \rightarrow \mu^+\mu^-)$. Using the known value $\mathcal{B}(b \rightarrow J/\psi X) = (1.16 \pm 0.10) \times 10^{-2}$ [12], one obtains

$$\mathcal{B}(b \rightarrow \psi(2S)X) = (3.08 \pm 0.02(\text{stat}) \pm 0.18(\text{syst}) \pm 0.27(\mathcal{B})) \times 10^{-3}.$$

This result is in agreement with the world-average value [12]. The $\mathcal{B}(b \rightarrow J/\psi X)$ uncertainty dominates the total uncertainty from the branching fractions.

7 Conclusions

The production cross-sections of $\psi(2S)$ mesons in proton-proton collisions at a centre-of-mass energy of 13 TeV are reported with a data sample corresponding to an integrated luminosity of $275 \pm 11 \text{ pb}^{-1}$, collected by the LHCb detector in 2015. The double-differential cross-sections, as functions of p_T and y of the $\psi(2S)$ meson in the range of $2 < p_T < 20 \text{ GeV}/c$ and $2.0 < y < 4.5$, are determined for prompt $\psi(2S)$ mesons and $\psi(2S)$ mesons from b -hadron decays. A new measurement of the branching fraction $\mathcal{B}(b \rightarrow \psi(2S)X)$ is presented, which is in agreement with the world average [12]. The measured prompt $\psi(2S)$ production cross-section as a function of transverse momentum is in good agreement in the high p_T region with theoretical calculations in the NRQCD framework. Theoretical predictions based on the FONLL calculations describe well the measured cross-sections for $\psi(2S)$ mesons from b -hadron decays.

A new measurement of $\psi(2S)$ production cross-sections at 7 TeV is performed using the 2011 data sample corresponding to an integrated luminosity of $614 \pm 11 \text{ pb}^{-1}$. The new

result provides a significantly reduced uncertainty compared to the previous independent LHCb result [18].

The cross section ratios between 13 TeV and 7 TeV show reasonable agreement with theoretical calculations.

Acknowledgements

We thank Kuang-Ta Chao and Yan-Qing Ma for frequent and interesting discussions on the production of $\psi(2S)$ mesons. We express our gratitude to our colleagues in the CERN accelerator departments for the excellent performance of the LHC. We thank the technical and administrative staff at the LHCb institutes. We acknowledge support from CERN and from the national agencies: CAPES, CNPq, FAPERJ and FINEP (Brazil); MOST and NSFC (China); CNRS/IN2P3 (France); BMBF, DFG and MPG (Germany); INFN (Italy); NWO (Netherlands); MNiSW and NCN (Poland); MEN/IFA (Romania); MSHE (Russia); MinECo (Spain); SNSF and SER (Switzerland); NASU (Ukraine); STFC (United Kingdom); DOE NP and NSF (USA). We acknowledge the computing resources that are provided by CERN, IN2P3 (France), KIT and DESY (Germany), INFN (Italy), SURF (Netherlands), PIC (Spain), GridPP (United Kingdom), RRCKI and Yandex LLC (Russia), CSCS (Switzerland), IFIN-HH (Romania), CBPF (Brazil), PL-GRID (Poland) and OSC (USA). We are indebted to the communities behind the multiple open-source software packages on which we depend. Individual groups or members have received support from AvH Foundation (Germany); EPLANET, Marie Skłodowska-Curie Actions and ERC (European Union); ANR, Labex P2IO and OCEVU, and Région Auvergne-Rhône-Alpes (France); Key Research Program of Frontier Sciences of CAS, CAS PIFI, and the Thousand Talents Program (China); RFBR, RSF and Yandex LLC (Russia); GVA, XuntaGal and GENCAT (Spain); the Royal Society and the Leverhulme Trust (United Kingdom).

Appendices

A Result tables

Table 2: Double-differential production cross-sections (in nb/(GeV/ c)) of prompt $\psi(2S)$ mesons at 13 TeV in bins of (p_T, y) . The first uncertainties are statistical, the second are the uncorrelated systematic uncertainties between bins, and the last are the correlated systematic uncertainties between bins. Adjacent bins with large statistical uncertainties have been merged.

p_T (GeV/ c)	2.0 < y < 2.5		2.5 < y < 3.0		3.0 < y < 3.5		3.5 < y < 4.0		4.0 < y < 4.5	
	2.0 < y < 2.5	2.5 < y < 3.0	2.5 < y < 3.0	3.0 < y < 3.5	3.0 < y < 3.5	3.5 < y < 4.0	3.5 < y < 4.0	4.0 < y < 4.5	4.0 < y < 4.5	
2–3	232.86 ± 5.80 ± 5.39 ± 18.24	228.46 ± 3.53 ± 1.65 ± 17.70	198.36 ± 2.86 ± 1.34 ± 15.33	167.07 ± 2.19 ± 1.30 ± 12.93	133.13 ± 1.99 ± 1.62 ± 10.42					
3–4	192.93 ± 3.96 ± 4.02 ± 9.74	166.62 ± 2.36 ± 1.27 ± 8.22	147.39 ± 1.90 ± 1.07 ± 7.25	120.42 ± 1.49 ± 0.96 ± 6.00	85.03 ± 1.42 ± 1.09 ± 4.37					
4–5	124.73 ± 2.38 ± 2.70 ± 9.15	108.56 ± 1.41 ± 0.88 ± 7.92	94.79 ± 1.09 ± 0.74 ± 6.90	76.73 ± 0.93 ± 0.68 ± 5.59	57.41 ± 1.00 ± 0.82 ± 4.28					
5–6	77.27 ± 1.46 ± 1.78 ± 4.89	66.05 ± 0.82 ± 0.59 ± 4.16	58.12 ± 0.65 ± 0.52 ± 3.65	47.25 ± 0.44 ± 0.48 ± 2.98	34.35 ± 0.66 ± 0.58 ± 2.29					
6–7	45.13 ± 0.91 ± 1.11 ± 4.73	41.43 ± 0.53 ± 0.43 ± 4.34	35.20 ± 0.43 ± 0.37 ± 3.69	28.70 ± 0.39 ± 0.36 ± 3.01	19.22 ± 0.47 ± 0.38 ± 2.08					
7–8	28.87 ± 0.62 ± 0.77 ± 1.95	25.38 ± 0.35 ± 0.32 ± 1.70	21.00 ± 0.30 ± 0.27 ± 1.41	15.97 ± 0.27 ± 0.25 ± 1.07	12.23 ± 0.32 ± 0.31 ± 0.91					
8–9	17.52 ± 0.42 ± 0.49 ± 1.19	15.39 ± 0.25 ± 0.24 ± 1.04	12.75 ± 0.22 ± 0.20 ± 0.86	9.86 ± 0.20 ± 0.19 ± 0.67	6.08 ± 0.21 ± 0.18 ± 0.47					
9–10	10.94 ± 0.29 ± 0.34 ± 0.56	9.63 ± 0.18 ± 0.18 ± 0.48	7.46 ± 0.16 ± 0.14 ± 0.38	5.90 ± 0.15 ± 0.15 ± 0.30	3.81 ± 0.16 ± 0.14 ± 0.26					
10–11	7.66 ± 0.23 ± 0.28 ± 0.50	5.98 ± 0.14 ± 0.13 ± 0.39	4.84 ± 0.13 ± 0.11 ± 0.31	3.83 ± 0.12 ± 0.11 ± 0.25	2.47 ± 0.11 ± 0.11 ± 0.19					
11–12	4.25 ± 0.16 ± 0.17 ± 0.23	3.86 ± 0.11 ± 0.10 ± 0.21	3.16 ± 0.10 ± 0.09 ± 0.17	2.37 ± 0.09 ± 0.08 ± 0.13	1.67 ± 0.10 ± 0.09 ± 0.13					
12–13	3.09 ± 0.13 ± 0.16 ± 0.27	2.44 ± 0.13 ± 0.07 ± 0.21	2.02 ± 0.08 ± 0.07 ± 0.18	1.39 ± 0.07 ± 0.06 ± 0.12	0.74 ± 0.06 ± 0.05 ± 0.07					
13–14	1.63 ± 0.09 ± 0.08 ± 0.12	1.57 ± 0.07 ± 0.06 ± 0.12	1.26 ± 0.06 ± 0.05 ± 0.09	0.91 ± 0.05 ± 0.04 ± 0.07	0.58 ± 0.06 ± 0.04 ± 0.05					
14–15	1.42 ± 0.08 ± 0.08 ± 0.07	1.26 ± 0.06 ± 0.05 ± 0.06	0.81 ± 0.05 ± 0.04 ± 0.04	0.59 ± 0.04 ± 0.04 ± 0.03	0.26 ± 0.03 ± 0.02 ± 0.02					
15–16	1.18 ± 0.08 ± 0.09 ± 0.06	0.86 ± 0.05 ± 0.04 ± 0.04	0.58 ± 0.04 ± 0.03 ± 0.03	0.41 ± 0.03 ± 0.02 ± 0.02	0.15 ± 0.01 ± 0.01 ± 0.01					
16–17	0.81 ± 0.06 ± 0.07 ± 0.04	0.59 ± 0.04 ± 0.03 ± 0.03	0.39 ± 0.03 ± 0.03 ± 0.02							
17–18	0.54 ± 0.05 ± 0.06 ± 0.03	0.42 ± 0.03 ± 0.03 ± 0.02								
18–19	0.29 ± 0.02 ± 0.02 ± 0.01	0.28 ± 0.02 ± 0.02 ± 0.02	0.21 ± 0.01 ± 0.01 ± 0.01							
19–20										

Table 3: Double-differential production cross-sections (in nb/(GeV/c)) of $\psi(2S)$ -from- b mesons at 13 TeV in bins of (p_T, y) . The first uncertainties are statistical, the second are the uncorrelated systematic uncertainties between bins, and the last are the correlated systematic uncertainties between bins. Adjacent bins with large statistical uncertainties have been merged.

p_T (GeV/c)	$2.0 < y < 2.5$	$2.5 < y < 3.0$	$3.0 < y < 3.5$	$3.5 < y < 4.0$	$4.0 < y < 4.5$
2–3	69.99 ± 1.94 ± 1.65 ± 5.51	61.15 ± 1.14 ± 0.48 ± 4.78	51.47 ± 0.97 ± 0.40 ± 3.99	37.86 ± 0.87 ± 0.35 ± 2.95	24.04 ± 0.94 ± 0.36 ± 1.89
3–4	56.37 ± 1.45 ± 1.17 ± 3.05	47.89 ± 0.83 ± 0.36 ± 2.45	39.58 ± 0.70 ± 0.31 ± 2.45	29.92 ± 0.64 ± 0.27 ± 1.57	19.49 ± 0.70 ± 0.29 ± 1.01
4–5	37.99 ± 1.00 ± 0.78 ± 2.80	34.38 ± 0.58 ± 0.25 ± 2.51	28.42 ± 0.48 ± 0.21 ± 2.08	21.25 ± 0.45 ± 0.19 ± 1.55	12.89 ± 0.50 ± 0.20 ± 0.97
5–6	27.93 ± 0.72 ± 0.60 ± 1.77	23.18 ± 0.40 ± 0.18 ± 1.46	19.18 ± 0.34 ± 0.15 ± 1.24	14.62 ± 0.24 ± 0.14 ± 0.94	7.94 ± 0.35 ± 0.14 ± 0.56
6–7	16.99 ± 0.49 ± 0.37 ± 1.78	15.74 ± 0.29 ± 0.13 ± 1.65	12.33 ± 0.24 ± 0.11 ± 1.29	8.91 ± 0.22 ± 0.10 ± 0.94	4.83 ± 0.25 ± 0.09 ± 0.52
7–8	12.29 ± 0.37 ± 0.28 ± 0.83	10.14 ± 0.21 ± 0.09 ± 0.68	7.77 ± 0.18 ± 0.08 ± 0.53	5.75 ± 0.17 ± 0.07 ± 0.39	3.41 ± 0.18 ± 0.08 ± 0.26
8–9	9.05 ± 0.29 ± 0.20 ± 0.62	6.84 ± 0.16 ± 0.07 ± 0.46	5.24 ± 0.14 ± 0.06 ± 0.36	3.56 ± 0.13 ± 0.05 ± 0.24	2.09 ± 0.13 ± 0.05 ± 0.16
9–10	6.12 ± 0.22 ± 0.13 ± 0.32	4.85 ± 0.13 ± 0.06 ± 0.24	3.60 ± 0.11 ± 0.05 ± 0.19	2.53 ± 0.10 ± 0.04 ± 0.13	1.50 ± 0.10 ± 0.05 ± 0.10
10–11	4.17 ± 0.16 ± 0.11 ± 0.27	3.38 ± 0.11 ± 0.05 ± 0.22	2.52 ± 0.09 ± 0.04 ± 0.16	1.63 ± 0.08 ± 0.03 ± 0.11	0.87 ± 0.06 ± 0.03 ± 0.07
11–12	2.90 ± 0.13 ± 0.07 ± 0.16	2.38 ± 0.09 ± 0.04 ± 0.13	1.66 ± 0.08 ± 0.03 ± 0.11	1.07 ± 0.06 ± 0.03 ± 0.06	0.65 ± 0.06 ± 0.03 ± 0.06
12–13	2.09 ± 0.11 ± 0.06 ± 0.19	1.68 ± 0.07 ± 0.03 ± 0.15	1.22 ± 0.06 ± 0.03 ± 0.11	0.78 ± 0.05 ± 0.02 ± 0.07	0.41 ± 0.05 ± 0.02 ± 0.04
13–14	1.39 ± 0.08 ± 0.04 ± 0.11	1.24 ± 0.06 ± 0.03 ± 0.09	0.76 ± 0.05 ± 0.02 ± 0.06	0.61 ± 0.04 ± 0.02 ± 0.05	0.29 ± 0.04 ± 0.02 ± 0.03
14–15	1.18 ± 0.07 ± 0.04 ± 0.06	0.82 ± 0.05 ± 0.02 ± 0.04	0.71 ± 0.05 ± 0.02 ± 0.04	0.42 ± 0.04 ± 0.02 ± 0.02	
15–16	0.84 ± 0.06 ± 0.03 ± 0.04	0.70 ± 0.05 ± 0.02 ± 0.04	0.42 ± 0.03 ± 0.01 ± 0.03		0.16 ± 0.02 ± 0.01 ± 0.02
16–17	0.62 ± 0.05 ± 0.02 ± 0.03	0.54 ± 0.04 ± 0.02 ± 0.03	0.34 ± 0.03 ± 0.01 ± 0.02	0.24 ± 0.02 ± 0.01 ± 0.02	
17–18	0.63 ± 0.05 ± 0.03 ± 0.04	0.41 ± 0.03 ± 0.02 ± 0.02			
18–19	0.32 ± 0.03 ± 0.01 ± 0.02	0.28 ± 0.02 ± 0.01 ± 0.02	0.21 ± 0.01 ± 0.01 ± 0.01	0.09 ± 0.01 ± 0.00 ± 0.01	0.07 ± 0.01 ± 0.00 ± 0.01
19–20					

Table 4: Double-differential production cross-section in nb/(GeV/ c) of prompt $\psi(2S)$ mesons at 7 TeV in bins of (p_T, y). The first uncertainty is statistical, the second is the uncorrelated systematic uncertainties shared between bins and the last is the correlated systematic uncertainties.

p_T (GeV/ c)	2 < y < 2.5	2.5 < y < 3	3 < y < 3.5	3.5 < y < 4	4 < y < 4.5
18	94.34 ± 2.49 ± 5.59 ± 8.65	109.85 ± 1.38 ± 2.50 ± 5.04	97.07 ± 0.99 ± 1.90 ± 4.33	77.87 ± 0.78 ± 1.51 ± 3.11	57.90 ± 0.80 ± 1.57 ± 2.09
	73.08 ± 1.21 ± 4.35 ± 4.40	75.42 ± 0.66 ± 1.32 ± 3.53	65.66 ± 0.47 ± 0.85 ± 2.64	53.33 ± 0.40 ± 0.88 ± 2.23	36.34 ± 0.40 ± 0.80 ± 1.30
	44.86 ± 0.71 ± 2.47 ± 2.24	43.26 ± 0.38 ± 1.04 ± 4.14	37.21 ± 0.30 ± 0.58 ± 1.54	31.96 ± 0.27 ± 0.86 ± 1.31	18.98 ± 0.26 ± 0.93 ± 0.65
	25.99 ± 0.45 ± 1.64 ± 2.58	24.94 ± 0.25 ± 0.63 ± 1.20	22.42 ± 0.21 ± 0.58 ± 0.86	17.86 ± 0.19 ± 0.61 ± 0.69	10.33 ± 0.17 ± 0.39 ± 0.50
	16.58 ± 0.30 ± 1.26 ± 1.04	15.21 ± 0.17 ± 0.41 ± 0.66	12.82 ± 0.14 ± 0.40 ± 0.50	9.98 ± 0.13 ± 0.33 ± 0.44	5.61 ± 0.12 ± 0.30 ± 0.26
	7.03 ± 0.14 ± 1.16 ± 0.35	9.02 ± 0.12 ± 0.39 ± 0.41	7.16 ± 0.10 ± 0.31 ± 0.33	5.05 ± 0.09 ± 0.28 ± 0.23	2.92 ± 0.08 ± 0.18 ± 0.15
	6.10 ± 0.14 ± 0.63 ± 0.28	5.26 ± 0.09 ± 0.26 ± 0.23	4.63 ± 0.08 ± 0.20 ± 0.18	3.16 ± 0.07 ± 0.20 ± 0.13	1.89 ± 0.07 ± 0.20 ± 0.12
	3.89 ± 0.11 ± 0.36 ± 0.23	3.03 ± 0.06 ± 0.17 ± 0.14	2.50 ± 0.05 ± 0.17 ± 0.11	1.93 ± 0.06 ± 0.18 ± 0.07	1.04 ± 0.05 ± 0.15 ± 0.06
	2.56 ± 0.08 ± 0.29 ± 0.13	2.30 ± 0.06 ± 0.35 ± 0.10	1.50 ± 0.04 ± 0.16 ± 0.13	1.46 ± 0.05 ± 0.25 ± 0.10	0.38 ± 0.02 ± 0.08 ± 0.02
	2.42 ± 0.10 ± 0.90 ± 0.11	1.12 ± 0.04 ± 0.09 ± 0.05	0.84 ± 0.03 ± 0.12 ± 0.04	0.58 ± 0.03 ± 0.08 ± 0.05	0.35 ± 0.03 ± 0.10 ± 0.04
13–14	0.85 ± 0.04 ± 0.16 ± 0.04	0.88 ± 0.03 ± 0.12 ± 0.11	0.60 ± 0.03 ± 0.09 ± 0.04	0.33 ± 0.02 ± 0.06 ± 0.02	0.07 ± 0.01 ± 0.02 ± 0.01

Table 5: Double-differential production cross-section in nb/(GeV/ c) of $\psi(2S)$ -from- b mesons at 7 TeV in bins of (p_T, y). The first uncertainties are statistical, the second are the uncorrelated systematic uncertainties shared between bins and the last are the correlated systematic uncertainties.

p_T (GeV/ c)	$2 < y < 2.5$	$2.5 < y < 3$	$3 < y < 3.5$	$3.5 < y < 4$	$4 < y < 4.5$
3.5–4	27.65 ± 1.10 ± 1.64 ± 2.86	24.88 ± 0.55 ± 0.44 ± 1.66	21.06 ± 0.42 ± 0.35 ± 0.98	16.01 ± 0.36 ± 0.43 ± 0.65	9.62 ± 0.36 ± 0.32 ± 0.53
4–5	20.85 ± 0.54 ± 1.12 ± 1.36	19.60 ± 0.29 ± 0.26 ± 1.14	15.58 ± 0.22 ± 0.19 ± 0.74	11.05 ± 0.19 ± 0.18 ± 0.46	6.58 ± 0.18 ± 0.18 ± 0.23
5–6	13.31 ± 0.36 ± 0.96 ± 0.93	13.04 ± 0.19 ± 0.19 ± 1.31	9.80 ± 0.15 ± 0.13 ± 0.43	6.90 ± 0.13 ± 0.12 ± 0.28	4.00 ± 0.13 ± 0.14 ± 0.14
6–7	8.77 ± 0.24 ± 0.45 ± 0.93	8.15 ± 0.14 ± 0.12 ± 0.40	6.20 ± 0.11 ± 0.09 ± 0.26	4.53 ± 0.10 ± 0.08 ± 0.18	2.01 ± 0.09 ± 0.08 ± 0.14
7–8	6.24 ± 0.18 ± 0.33 ± 0.41	4.96 ± 0.10 ± 0.08 ± 0.25	4.02 ± 0.08 ± 0.07 ± 0.16	2.64 ± 0.07 ± 0.05 ± 0.15	1.38 ± 0.07 ± 0.06 ± 0.07
8–9	3.68 ± 0.12 ± 0.19 ± 0.23	3.40 ± 0.08 ± 0.07 ± 0.16	2.69 ± 0.07 ± 0.05 ± 0.14	1.61 ± 0.05 ± 0.04 ± 0.08	0.76 ± 0.05 ± 0.04 ± 0.04
9–10	3.14 ± 0.11 ± 0.21 ± 0.19	2.15 ± 0.06 ± 0.04 ± 0.09	1.33 ± 0.05 ± 0.04 ± 0.12	1.00 ± 0.04 ± 0.03 ± 0.04	0.37 ± 0.03 ± 0.02 ± 0.04
10–11	1.96 ± 0.08 ± 0.12 ± 0.12	1.46 ± 0.05 ± 0.04 ± 0.07	1.11 ± 0.04 ± 0.04 ± 0.07	0.66 ± 0.03 ± 0.02 ± 0.03	0.32 ± 0.03 ± 0.02 ± 0.02
11–12	1.28 ± 0.06 ± 0.07 ± 0.07	1.00 ± 0.04 ± 0.03 ± 0.05	0.75 ± 0.03 ± 0.03 ± 0.07	0.42 ± 0.02 ± 0.02 ± 0.03	0.18 ± 0.02 ± 0.02 ± 0.01
12–13	0.80 ± 0.04 ± 0.05 ± 0.05	0.73 ± 0.03 ± 0.02 ± 0.04	0.51 ± 0.03 ± 0.02 ± 0.02	0.28 ± 0.02 ± 0.01 ± 0.03	0.09 ± 0.02 ± 0.01 ± 0.01
13–14	0.66 ± 0.04 ± 0.07 ± 0.04	0.51 ± 0.03 ± 0.02 ± 0.06	0.33 ± 0.02 ± 0.01 ± 0.02	0.17 ± 0.02 ± 0.01 ± 0.01	0.06 ± 0.01 ± 0.01 ± 0.01

Table 6: Differential production cross-sections $d\sigma/dp_T$ (in nb/(GeV/c)) of prompt $\psi(2S)$ and $\psi(2S)$ -from- b mesons at 13 TeV. The first uncertainties are statistical and the second (third) are uncorrelated (correlated) systematic uncertainties amongst bins.

p_T (GeV/c)	Prompt $\psi(2S)$	$\psi(2S)$ -from- b
2–3	$479.94 \pm 3.97 \pm 3.08 \pm 37.31$	$122.26 \pm 1.38 \pm 0.91 \pm 9.56$
3–4	$356.19 \pm 2.69 \pm 2.29 \pm 17.79$	$96.62 \pm 1.02 \pm 0.66 \pm 5.27$
4–5	$231.12 \pm 1.64 \pm 1.56 \pm 16.92$	$67.47 \pm 0.71 \pm 0.45 \pm 4.95$
5–6	$141.52 \pm 0.98 \pm 1.04 \pm 8.99$	$46.43 \pm 0.49 \pm 0.34 \pm 2.98$
6–7	$84.84 \pm 0.65 \pm 0.68 \pm 8.92$	$29.40 \pm 0.35 \pm 0.21 \pm 3.10$
7–8	$51.72 \pm 0.44 \pm 0.48 \pm 3.52$	$19.68 \pm 0.26 \pm 0.16 \pm 1.34$
8–9	$30.80 \pm 0.30 \pm 0.32 \pm 2.11$	$13.38 \pm 0.20 \pm 0.12 \pm 0.92$
9–10	$18.87 \pm 0.22 \pm 0.23 \pm 0.99$	$9.29 \pm 0.16 \pm 0.08 \pm 0.49$
10–11	$12.39 \pm 0.17 \pm 0.18 \pm 0.82$	$6.29 \pm 0.12 \pm 0.07 \pm 0.42$
11–12	$7.65 \pm 0.13 \pm 0.13 \pm 0.44$	$4.33 \pm 0.10 \pm 0.05 \pm 0.26$
12–13	$4.84 \pm 0.11 \pm 0.10 \pm 0.43$	$3.09 \pm 0.08 \pm 0.04 \pm 0.28$
13–14	$2.98 \pm 0.07 \pm 0.06 \pm 0.23$	$2.14 \pm 0.06 \pm 0.03 \pm 0.17$
14–20	$1.13 \pm 0.02 \pm 0.02 \pm 0.06$	$0.90 \pm 0.02 \pm 0.01 \pm 0.05$

Table 7: Differential production cross-sections $d\sigma/dy$ (in nb) of prompt $\psi(2S)$ and $\psi(2S)$ -from- b mesons at 13 TeV per rapidity unit. The first uncertainties are statistical and the second (third) are uncorrelated (correlated) systematic uncertainties amongst bins.

y	Prompt $\psi(2S)$	$\psi(2S)$ -from- b
2.0–2.5	$751.4 \pm 7.7 \pm 7.6 \pm 51.8$	$251.2 \pm 2.8 \pm 2.3 \pm 17.6$
2.5–3.0	$679.1 \pm 4.6 \pm 2.4 \pm 46.7$	$215.9 \pm 1.6 \pm 0.7 \pm 15.0$
3.0–3.5	$588.7 \pm 3.7 \pm 2.0 \pm 40.4$	$175.8 \pm 1.4 \pm 0.6 \pm 12.7$
3.5–4.0	$482.3 \pm 2.9 \pm 1.9 \pm 33.2$	$129.6 \pm 1.2 \pm 0.5 \pm 9.1$
4.0–4.5	$357.8 \pm 2.8 \pm 2.3 \pm 25.6$	$79.0 \pm 1.4 \pm 0.5 \pm 5.7$

Table 8: Differential cross-sections $d\sigma/dp_T$ (in nb/(GeV/c)) of prompt $\psi(2S)$ and $\psi(2S)$ -from- b mesons at 7 TeV, integrated over y between 2.0 and 4.5. The first uncertainties are statistical and the second (third) are uncorrelated (correlated) systematic uncertainties amongst bins.

p_T (GeV/c)	Prompt $\psi(2S)$	$\psi(2S)$ -from- b
3.5–4	$218.52 \pm 1.61 \pm 3.38 \pm 11.61$	$49.61 \pm 0.70 \pm 0.91 \pm 3.34$
4–5	$151.91 \pm 0.78 \pm 2.39 \pm 7.05$	$36.83 \pm 0.35 \pm 0.60 \pm 1.97$
5–6	$88.13 \pm 0.47 \pm 1.51 \pm 4.94$	$23.52 \pm 0.24 \pm 0.50 \pm 1.55$
6–7	$50.77 \pm 0.30 \pm 0.99 \pm 2.92$	$14.83 \pm 0.16 \pm 0.24 \pm 0.95$
7–8	$30.10 \pm 0.21 \pm 0.73 \pm 1.45$	$9.62 \pm 0.12 \pm 0.18 \pm 0.52$
8–9	$15.59 \pm 0.12 \pm 0.65 \pm 0.74$	$6.08 \pm 0.09 \pm 0.11 \pm 0.32$
9–10	$10.52 \pm 0.10 \pm 0.38 \pm 0.47$	$3.99 \pm 0.07 \pm 0.11 \pm 0.24$
10–11	$6.20 \pm 0.08 \pm 0.25 \pm 0.30$	$2.75 \pm 0.05 \pm 0.07 \pm 0.16$
11–12	$4.10 \pm 0.06 \pm 0.27 \pm 0.24$	$1.81 \pm 0.04 \pm 0.04 \pm 0.12$
12–13	$2.65 \pm 0.06 \pm 0.46 \pm 0.15$	$1.20 \pm 0.03 \pm 0.03 \pm 0.08$
13–14	$1.37 \pm 0.03 \pm 0.12 \pm 0.11$	$0.86 \pm 0.03 \pm 0.04 \pm 0.07$

Table 9: Differential cross-sections $d\sigma/dy$ (in nb) of prompt $\psi(2S)$ and $\psi(2S)$ -from- b mesons at 7 TeV, integrated over p_T between 3.5 and 14 GeV/ c . The first uncertainties are statistical and the second (third) are uncorrelated (correlated) systematic uncertainties amongst bins.

y	Prompt $\psi(2S)$	$\psi(2S)$ -from- b
2.0–2.5	$230.5 \pm 2.0 \pm 6.3 \pm 15.7$	$74.5 \pm 0.9 \pm 1.8 \pm 5.8$
2.5–3.0	$235.4 \pm 1.1 \pm 2.3 \pm 13.1$	$67.4 \pm 0.5 \pm 0.4 \pm 4.4$
3.0–3.5	$203.9 \pm 0.8 \pm 1.6 \pm 8.5$	$52.8 \pm 0.4 \pm 0.3 \pm 2.5$
3.5–4.0	$164.6 \pm 0.7 \pm 1.7 \pm 6.8$	$37.3 \pm 0.3 \pm 0.3 \pm 1.6$
4.0–4.5	$106.9 \pm 0.7 \pm 1.6 \pm 4.2$	$20.6 \pm 0.3 \pm 0.3 \pm 1.0$

Table 10: Fractions of $\psi(2S)$ -from- b (in %) at 13 TeV in bins of (p_T, y) of $\psi(2S)$ mesons. The uncertainties are statistical only. The systematic uncertainties are negligible. Adjacent bins with large statistical uncertainty have been merged.

p_T (GeV/ c)	$2.0 < y < 2.5$	$2.5 < y < 3.0$	$3.0 < y < 3.5$	$3.5 < y < 4.0$	$4.0 < y < 4.5$
2–3	23.0 ± 0.6	20.8 ± 0.4	20.4 ± 0.4	18.1 ± 0.4	14.8 ± 0.5
3–4	22.4 ± 0.6	22.2 ± 0.4	21.0 ± 0.4	19.5 ± 0.4	18.4 ± 0.6
4–5	23.0 ± 0.6	23.9 ± 0.4	22.8 ± 0.4	21.4 ± 0.4	18.8 ± 0.7
5–6	25.9 ± 0.6	25.5 ± 0.4	24.4 ± 0.4	22.8 ± 0.5	18.5 ± 0.7
6–7	27.1 ± 0.7	27.1 ± 0.5	25.6 ± 0.5	23.3 ± 0.5	20.2 ± 1.0
7–8	29.8 ± 0.8	28.7 ± 0.5	26.4 ± 0.6	25.8 ± 0.7	22.1 ± 1.0
8–9	32.8 ± 0.9	30.6 ± 0.6	28.8 ± 0.7	26.6 ± 0.8	25.3 ± 1.4
9–10	34.2 ± 1.0	32.8 ± 0.8	32.4 ± 0.9	29.7 ± 1.0	28.7 ± 1.7
10–11	35.5 ± 1.2	35.4 ± 0.9	33.7 ± 1.1	29.7 ± 1.2	26.9 ± 1.8
11–12	38.5 ± 1.5	37.6 ± 1.1	34.8 ± 1.4	30.6 ± 1.6	28.1 ± 2.4
12–13	40.7 ± 1.7	38.7 ± 1.4	36.4 ± 1.5	34.3 ± 2.0	31.7 ± 3.4
13–14	42.1 ± 2.1	41.8 ± 1.6	35.9 ± 1.9	37.6 ± 1.0	31.2 ± 3.9
14–15	44.2 ± 2.1	39.4 ± 1.8	44.7 ± 2.2	36.4 ± 2.8	39.2 ± 1.7
15–16	43.4 ± 2.5	42.5 ± 2.1	41.5 ± 1.0	36.8 ± 2.6	
16–17	43.6 ± 2.8	45.9 ± 2.5	44.8 ± 1.3		
17–18	51.7 ± 3.1	47.1 ± 3.0			
18–19	49.7 ± 3.2	49.1 ± 2.5	47.2 ± 2.5	34.7 ± 3.6	29.0 ± 3.9
19–20					

Table 11: Fractions of $\psi(2S)$ -from- b (in %) at 7 TeV in bins of (p_T, y) of $\psi(2S)$ mesons. The uncertainties are statistical only. The systematic uncertainties are negligible.

p_T (GeV/ c)	$2.0 < y < 2.5$	$2.5 < y < 3.0$	$3.0 < y < 3.5$	$3.5 < y < 4.0$	$4.0 < y < 4.5$
3.5–4	21.11 ± 0.79	17.91 ± 0.37	17.26 ± 0.33	16.52 ± 0.34	13.93 ± 0.50
4–5	21.73 ± 0.53	20.21 ± 0.28	18.42 ± 0.25	16.95 ± 0.27	15.47 ± 0.40
5–6	22.15 ± 0.55	22.40 ± 0.31	20.08 ± 0.29	17.89 ± 0.32	16.49 ± 0.50
6–7	24.12 ± 0.61	24.49 ± 0.37	21.45 ± 0.35	20.21 ± 0.41	16.18 ± 0.65
7–8	27.34 ± 0.68	25.04 ± 0.44	23.81 ± 0.44	21.64 ± 0.52	18.48 ± 0.83
8–9	28.44 ± 0.80	27.26 ± 0.54	26.81 ± 0.57	23.68 ± 0.70	19.12 ± 1.10
9–10	30.46 ± 0.08	29.40 ± 0.68	21.50 ± 0.69	24.95 ± 0.88	17.28 ± 1.38
10–11	32.97 ± 1.08	31.67 ± 0.83	28.14 ± 0.87	27.30 ± 1.17	24.10 ± 1.77
11–12	34.86 ± 1.33	33.31 ± 1.02	30.98 ± 1.16	28.55 ± 1.44	27.33 ± 2.10
12–13	35.56 ± 1.62	37.85 ± 1.31	33.30 ± 1.44	28.50 ± 1.78	20.81 ± 3.01
13–14	38.79 ± 1.93	36.68 ± 1.51	34.21 ± 1.80	30.97 ± 2.50	36.20 ± 6.19

Table 12: Ratios of production cross-sections at 13 TeV between $\psi(2S)$ mesons and J/ψ mesons in bins of p_T for prompt production and for those from b -hadron decays integrated in the rapidity range $2.0 < y < 4.5$. The statistical and systematic uncertainties are added in quadrature.

p_T (GeV/ c)	Prompt	From b -hadron decays
2–3	0.135 ± 0.010	0.241 ± 0.018
3–4	0.158 ± 0.007	0.263 ± 0.013
4–5	0.182 ± 0.012	0.278 ± 0.019
5–6	0.201 ± 0.011	0.317 ± 0.018
6–7	0.225 ± 0.023	0.311 ± 0.031
7–8	0.259 ± 0.016	0.341 ± 0.021
8–9	0.271 ± 0.017	0.374 ± 0.024
9–10	0.284 ± 0.012	0.365 ± 0.018
10–11	0.310 ± 0.019	0.370 ± 0.025
11–12	0.305 ± 0.017	0.357 ± 0.023
12–13	0.315 ± 0.029	0.380 ± 0.037
13–14	0.294 ± 0.026	0.361 ± 0.033

Table 13: Ratios of production cross-sections between $\psi(2S)$ mesons and J/ψ mesons at 13 TeV in bins of y for prompt production and for those from b -hadron decays integrated in the transverse momentum range $2 < p_T < 14$ GeV/ c . The statistical and systematic uncertainties are added in quadrature.

y	Prompt	From b -hadron decays
2.0–2.5	0.175 ± 0.011	0.288 ± 0.018
2.5–3.0	0.168 ± 0.010	0.289 ± 0.017
3.0–3.5	0.164 ± 0.009	0.279 ± 0.017
3.5–4.0	0.159 ± 0.010	0.261 ± 0.017
4.0–4.5	0.150 ± 0.012	0.237 ± 0.019

Table 14: Ratios of production cross-sections between 13 TeV and 7 TeV in bins of p_T for prompt $\psi(2S)$ and $\psi(2S)$ -from- b mesons integrated in the rapidity range $2.0 < y < 4.5$. The statistical and systematic uncertainties are added in quadrature.

p_T (GeV/ c)	Prompt $\psi(2S)$	$\psi(2S)$ -from- b
3.5–4	1.63 ± 0.09	1.95 ± 0.13
4–5	1.52 ± 0.12	1.83 ± 0.15
5–6	1.61 ± 0.11	1.97 ± 0.15
6–7	1.67 ± 0.19	1.98 ± 0.23
7–8	1.72 ± 0.12	2.05 ± 0.14
8–9	1.97 ± 0.13	2.20 ± 0.15
9–10	1.79 ± 0.08	2.33 ± 0.14
10–11	2.00 ± 0.13	2.28 ± 0.17
11–12	1.87 ± 0.12	2.39 ± 0.15
12–13	1.83 ± 0.20	2.57 ± 0.24
13–14	2.18 ± 0.25	2.49 ± 0.27

Table 15: Ratios of cross-sections between measurements at 13 TeV and 7 TeV in different bins of y for prompt $\psi(2S)$ and $\psi(2S)$ -from- b mesons integrated in the transverse momentum range $3.5 < p_T < 14$ GeV/ c . The statistical and systematic uncertainties are added in quadrature.

y	Prompt $\psi(2S)$	$\psi(2S)$ -from- b
2.0–2.5	1.81 ± 0.14	2.00 ± 0.17
2.5–3.0	1.54 ± 0.11	1.89 ± 0.14
3.0–3.5	1.54 ± 0.10	1.94 ± 0.13
3.5–4.0	1.54 ± 0.10	2.03 ± 0.13
4.0–4.5	1.69 ± 0.10	2.17 ± 0.14

B Scaling factors for alternative polarisation scenarios

Table 16: Multiplicative scaling factors needed to obtain the prompt $\psi(2S)$ differential cross-sections from unpolarised cross-section measurements at 13 TeV as reported in Table 2 under the assumption of fully transverse polarisation ($\alpha = +1$).

p_T (GeV/c)	$2.0 < y < 2.5$	$2.5 < y < 3.0$	$3.0 < y < 3.5$	$3.5 < y < 4.0$	$4.0 < y < 4.5$
2–3	1.084	1.081	0.997	0.984	0.993
3–4	1.202	1.047	0.964	0.950	0.948
4–5	1.164	1.034	0.961	0.937	0.921
5–6	1.138	1.016	0.959	0.940	0.922
6–7	1.100	1.012	0.970	0.939	0.923
7–8	1.110	0.996	0.965	0.937	0.915
8–9	1.120	0.993	0.962	0.943	0.937
9–10	1.037	0.985	0.962	0.940	0.941
10–11	1.070	0.941	0.941	0.960	0.910
11–12	1.022	0.952	0.958	0.926	0.925
12–13	1.096	0.940	0.932	0.944	0.897
13–14	1.007	0.964	0.949	0.932	0.924
14–15	1.060	0.944	0.939	0.924	0.909
15–16	0.932	0.940	0.910	0.931	
16–17	1.051	0.932	0.930		
17–18	1.080	0.946			0.850
18–19	0.969	0.934	0.924	0.911	
19–20					

Table 17: Multiplicative scaling factors needed to obtain the prompt $\psi(2S)$ differential cross-sections from unpolarised cross-section measurements at 13 TeV as reported in Table 2 under the assumption of fully longitudinal polarisation ($\alpha = -1$).

p_T (GeV/c)	$2.0 < y < 2.5$	$2.5 < y < 3.0$	$3.0 < y < 3.5$	$3.5 < y < 4.0$	$4.0 < y < 4.5$
2–3	0.846	0.870	0.987	1.016	1.008
3–4	0.754	0.909	1.039	1.079	1.092
4–5	0.777	0.934	1.053	1.092	1.123
5–6	0.806	0.950	1.051	1.091	1.132
6–7	0.829	0.958	1.040	1.069	1.129
7–8	0.843	0.977	1.041	1.079	1.102
8–9	0.865	0.992	1.054	1.073	1.120
9–10	0.908	1.004	1.061	1.066	1.129
10–11	0.882	1.024	1.068	1.098	1.096
11–12	0.944	1.035	1.077	1.069	1.114
12–13	0.941	1.050	1.079	1.076	1.126
13–14	0.992	1.069	1.067	1.100	1.115
14–15	0.966	1.076	1.085	1.114	1.143
15–16	0.964	1.082	1.142	1.102	—
16–17	1.011	1.099	1.102	—	—
17–18	0.992	1.074	—	—	—
18–19	1.037	1.094	1.114	1.140	1.013
19–20	—	—	—	—	—

Table 18: Multiplicative scaling factors needed to obtain the prompt $\psi(2S)$ differential cross-sections from unpolarised cross-section measurements at 13 TeV as reported in Table 2 under the assumption of 20 % longitudinal polarisation ($\alpha = -0.2$), corresponding to a conservative limit of the $\psi(2S)$ polarisation measured at 7 TeV [53].

p_T (GeV/c)	$2.0 < y < 2.5$	$2.5 < y < 3.0$	$3.0 < y < 3.5$	$3.5 < y < 4.0$	$4.0 < y < 4.5$
2–3	0.975	0.976	0.997	1.001	0.998
3–4	0.955	0.983	1.005	1.013	1.012
4–5	0.955	0.990	1.010	1.012	1.012
5–6	0.963	0.988	1.007	1.014	1.018
6–7	0.960	0.990	1.008	1.004	1.020
7–8	0.976	0.991	1.006	1.007	1.004
8–9	0.993	0.998	1.010	1.008	1.025
9–10	0.973	0.998	1.013	1.003	1.033
10–11	0.981	0.984	1.004	1.030	0.999
11–12	0.986	0.996	1.019	0.996	1.016
12–13	1.023	0.995	1.004	1.010	1.005
13–14	1.005	1.021	1.008	1.014	1.016
14–15	1.024	1.010	1.011	1.016	
15–16	0.948	1.011	1.020		1.019
16–17	1.049	1.013	1.013		
17–18	1.086	1.009			
18–19	1.004	1.013	1.015	1.019	0.929
19–20					

Table 19: Multiplicative scaling factors needed to obtain the prompt $\psi(2S)$ differential cross-sections from unpolarised cross-section measurements at 7 TeV as reported in Table 4 under the assumption of fully transverse polarisation ($\alpha = +1$).

p_T (GeV/c)	$2.0 < y < 2.5$	$2.5 < y < 3.0$	$3.0 < y < 3.5$	$3.5 < y < 4.0$	$4.0 < y < 4.5$
3.5–4	1.087	1.288	1.164	1.111	1.079
4–5	1.435	1.260	1.157	1.103	1.067
5–6	1.397	1.231	1.156	1.102	1.066
6–7	1.362	1.220	1.144	1.102	1.071
7–8	1.305	1.186	1.142	1.097	1.072
8–9	1.287	1.184	1.114	1.088	1.074
9–10	1.250	1.150	1.124	1.086	1.071
10–11	1.350	1.218	1.188	1.162	1.106
11–12	1.347	1.209	1.091	1.143	1.085
12–13	1.246	1.222	1.127	1.139	1.103
13–14	1.253	1.162	1.181	1.115	1.057

Table 20: Multiplicative scaling factors needed to obtain the prompt $\psi(2S)$ differential cross-sections from unpolarised cross-section measurements at 7 TeV as reported in Table 4 under the assumption of fully longitudinal polarisation ($\alpha = -1$).

p_T (GeV/c)	$2.0 < y < 2.5$	$2.5 < y < 3.0$	$3.0 < y < 3.5$	$3.5 < y < 4.0$	$4.0 < y < 4.5$
3.5–4	0.858	0.673	0.784	0.847	0.893
4–5	0.583	0.697	0.792	0.854	0.908
5–6	0.596	0.716	0.788	0.851	0.906
6–7	0.616	0.726	0.802	0.851	0.893
7–8	0.627	0.734	0.780	0.837	0.874
8–9	0.647	0.734	0.814	0.850	0.877
9–10	0.676	0.769	0.808	0.846	0.873
10–11	0.743	0.821	0.833	0.868	0.896
11–12	0.745	0.845	0.940	0.879	0.882
12–13	0.769	0.820	0.874	0.861	0.908
13–14	0.802	0.872	0.834	0.922	0.947

Table 21: Multiplicative scaling factors needed to obtain the prompt $\psi(2S)$ differential cross-sections from unpolarised cross-section measurements at 7 TeV as reported in Table 4 under the assumption of 20 % longitudinal polarisation ($\alpha = -0.2$), corresponding to a conservative limit of the $\psi(2S)$ polarisation measured at 7 TeV [53]

p_T (GeV/c)	$2.0 < y < 2.5$	$2.5 < y < 3.0$	$3.0 < y < 3.5$	$3.5 < y < 4.0$	$4.0 < y < 4.5$
3.5–4	0.980	0.944	0.967	0.979	0.986
4–5	0.922	0.949	0.969	0.980	0.989
5–6	0.923	0.951	0.967	0.979	0.988
6–7	0.928	0.953	0.969	0.978	0.986
7–8	0.917	0.945	0.957	0.969	0.978
8–9	0.928	0.944	0.963	0.972	0.980
9–10	0.930	0.953	0.963	0.969	0.977
10–11	1.013	1.014	1.007	1.017	1.008
11–12	1.016	1.023	1.020	1.013	0.988
12–13	0.991	1.013	1.003	1.001	1.010
13–14	1.011	1.018	1.003	1.022	1.005

References

- [1] A. Andronic *et al.*, *Heavy-flavour and quarkonium production in the LHC era: From proton-proton to heavy-ion collisions*, Eur. Phys. J. **C76** (2016) 107, arXiv:1506.03981.
- [2] N. Brambilla *et al.*, *Heavy quarkonium: Progress, puzzles, and opportunities*, Eur. Phys. J. **C71** (2011) 1534, arXiv:1010.5827.
- [3] C. E. Carlson and R. Suaya, *Hadronic production of the ψ/J meson*, Phys. Rev. **D14** (1976) 3115.
- [4] A. Donnachie and P. V. Landshoff, *Production of lepton pairs, J/ψ and charm with hadron beams*, Nucl. Phys. **B112** (1976) 233.
- [5] S. D. Ellis, M. B. Einhorn, and C. Quigg, *Comment on hadronic production of Psions*, Phys. Rev. Lett. **36** (1976) 1263.
- [6] H. Fritzsch, *Producing heavy quark flavors in hadronic collisions - a test of quantum chromodynamics*, Phys. Lett. **B67** (1977) 217.
- [7] M. Glück, J. F. Owens, and E. Reya, *Gluon contribution to hadronic J/ψ production*, Phys. Rev. **D17** (1978) 2324.
- [8] C.-H. Chang, *Hadronic production of J/ψ associated with a gluon*, Nucl. Phys. **B172** (1980) 425.
- [9] R. Baier and R. Rückl, *Hadronic production of J/ψ and Υ : transverse momentum distributions*, Phys. Lett. **B102** (1981) 364.
- [10] G. T. Bodwin, E. Braaten, and G. P. Lepage, *Rigorous QCD analysis of inclusive annihilation and production of heavy quarkonium*, Phys. Rev. **D51** (1995) 1125, Erratum ibid. **D55** (1997) 5853, arXiv:hep-ph/9407339.
- [11] P. Cho and A. K. Leibovich, *Color-octet quarkonia production*, Phys. Rev. **D53** (1996) 150, arXiv:hep-ph/9505329; P. Cho and A. K. Leibovich, *Color-octet quarkonia production. II*, Phys. Rev. **D53** (1996) 6203, arXiv:hep-ph/9511315.
- [12] Particle Data Group, M. Tanabashi *et al.*, *Review of particle physics*, Phys. Rev. **D98** (2018) 030001.
- [13] LHCb collaboration, R. Aaij *et al.*, *Observation of J/ψ -pair production in pp collisions at $\sqrt{s} = 7 \text{ TeV}$* , Phys. Lett. **B707** (2012) 52, arXiv:1109.0963.
- [14] LHCb collaboration, R. Aaij *et al.*, *Observation of double charm production involving open charm in pp collisions at $\sqrt{s} = 7 \text{ TeV}$* , JHEP **06** (2012) 141, Addendum ibid. **03** (2014) 108, arXiv:1205.0975.
- [15] CDF collaboration, F. Abe *et al.*, *J/ψ and $\psi(2S)$ production in $p\bar{p}$ collisions at $\sqrt{s} = 1.8 \text{ TeV}$* , Phys. Rev. Lett. **79** (1997) 572.

- [16] CDF collaboration, T. Aaltonen *et al.*, *Production of $\psi(2S)$ mesons in $p\bar{p}$ collisions at 1.96 TeV*, Phys. Rev. **D80** (2009) 031103, [arXiv:0905.1982](#).
- [17] CMS collaboration, S. Chatrchyan *et al.*, *J/ψ and $\psi(2S)$ production in pp collisions at $\sqrt{s} = 7$ TeV*, JHEP **02** (2012) 011, [arXiv:1111.1557](#).
- [18] LHCb collaboration, R. Aaij *et al.*, *Measurement of $\psi(2S)$ meson production in pp collisions at $\sqrt{s} = 7$ TeV*, Eur. Phys. J. **C72** (2012) 2100, Erratum *ibid.* **C80** (2020) 49, [arXiv:1204.1258](#).
- [19] ALICE collaboration, B. Abelev *et al.*, *Measurement of quarkonium production at forward rapidity in pp collisions at $\sqrt{s} = 7$ TeV*, Eur. Phys. J. **C74** (2014) 2974, [arXiv:1403.3648](#).
- [20] ATLAS collaboration, G. Aad *et al.*, *Measurement of the production cross-section of $\psi(2S) \rightarrow J/\psi (\rightarrow \mu^+ \mu^-) \pi^+ \pi^-$ in pp collisions at $\sqrt{s} = 7$ TeV at ATLAS*, JHEP **09** (2014) 079, [arXiv:1407.5532](#).
- [21] CMS collaboration, V. Khachatryan *et al.*, *Measurement of J/ψ and $\psi(2S)$ prompt double-differential cross sections in pp collisions at $\sqrt{s}=7$ TeV*, Phys. Rev. Lett. **114** (2015) 191802, [arXiv:1502.04155](#).
- [22] ATLAS collaboration, G. Aad *et al.*, *Measurement of the differential cross-sections of prompt and non-prompt production of J/ψ and $\psi(2S)$ in pp collisions at $\sqrt{s} = 7$ and 8 TeV with the ATLAS detector*, Eur. Phys. J. **C76** (2016) 283, [arXiv:1512.03657](#).
- [23] CMS collaboration, A. M. Sirunyan *et al.*, *Measurement of quarkonium production cross sections in pp collisions at $\sqrt{s} = 13$ TeV*, Phys. Lett. **B780** (2018) 251, [arXiv:1710.11002](#).
- [24] LHCb collaboration, R. Aaij *et al.*, *Measurement of forward J/ψ production cross-sections in pp collisions at $\sqrt{s} = 13$ TeV*, JHEP **10** (2015) 172, Erratum *ibid.* **05** (2017) 063, [arXiv:1509.00771](#).
- [25] LHCb collaboration, A. A. Alves Jr. *et al.*, *The LHCb detector at the LHC*, JINST **3** (2008) S08005.
- [26] LHCb collaboration, R. Aaij *et al.*, *LHCb detector performance*, Int. J. Mod. Phys. **A30** (2015) 1530022, [arXiv:1412.6352](#).
- [27] R. Aaij *et al.*, *Performance of the LHCb Vertex Locator*, JINST **9** (2014) P09007, [arXiv:1405.7808](#).
- [28] R. Arink *et al.*, *Performance of the LHCb Outer Tracker*, JINST **9** (2014) P01002, [arXiv:1311.3893](#).
- [29] P. d'Argent *et al.*, *Improved performance of the LHCb Outer Tracker in LHC Run 2*, JINST **9** (2017) P11016, [arXiv:1708.00819](#).
- [30] M. Adinolfi *et al.*, *Performance of the LHCb RICH detector at the LHC*, Eur. Phys. J. **C73** (2013) 2431, [arXiv:1211.6759](#).

- [31] A. A. Alves Jr. *et al.*, *Performance of the LHCb muon system*, JINST **8** (2013) P02022, [arXiv:1211.1346](https://arxiv.org/abs/1211.1346).
- [32] R. Aaij *et al.*, *The LHCb trigger and its performance in 2011*, JINST **8** (2013) P04022, [arXiv:1211.3055](https://arxiv.org/abs/1211.3055).
- [33] T. Sjöstrand, S. Mrenna, and P. Skands, *A brief introduction to PYTHIA 8.1*, Comput. Phys. Commun. **178** (2008) 852, [arXiv:0710.3820](https://arxiv.org/abs/0710.3820).
- [34] T. Sjöstrand, S. Mrenna, and P. Skands, *PYTHIA 6.4 physics and manual*, JHEP **05** (2006) 026, [arXiv:hep-ph/0603175](https://arxiv.org/abs/hep-ph/0603175).
- [35] I. Belyaev *et al.*, *Handling of the generation of primary events in Gauss, the LHCb simulation framework*, J. Phys. Conf. Ser. **331** (2011) 032047.
- [36] D. J. Lange, *The EvtGen particle decay simulation package*, Nucl. Instrum. Meth. **A462** (2001) 152.
- [37] P. Golonka and Z. Was, *PHOTOS Monte Carlo: A precision tool for QED corrections in Z and W decays*, Eur. Phys. J. **C45** (2006) 97, [arXiv:hep-ph/0506026](https://arxiv.org/abs/hep-ph/0506026).
- [38] M. Bargiotti and V. Vagnoni, *Heavy Quarkonia sector in PYTHIA 6.324: tuning, validation and perspectives at LHC(b)*, Jun, 2007. LHCb-2007-042. CERN-LHCb-2007-042.
- [39] Geant4 collaboration, J. Allison *et al.*, *Geant4 developments and applications*, IEEE Trans. Nucl. Sci. **53** (2006) 270; Geant4 collaboration, S. Agostinelli *et al.*, *Geant4: A simulation toolkit*, Nucl. Instrum. Meth. **A506** (2003) 250.
- [40] M. Clemencic *et al.*, *The LHCb simulation application, Gauss: Design, evolution and experience*, J. Phys. Conf. Ser. **331** (2011) 032023.
- [41] G. Dujany and B. Storaci, *Real-time alignment and calibration of the LHCb Detector in Run II*, J. Phys. Conf. Ser. **664** (2015) 082010.
- [42] W. Qian, *J/ψ production study at the LHCb experiment*, PhD thesis, Tsinghua University, Beijing, 2010, CERN-THESIS-2010-307.
- [43] LHCb collaboration, R. Aaij *et al.*, *Precision luminosity measurements at LHCb*, JINST **9** (2014) P12005, [arXiv:1410.0149](https://arxiv.org/abs/1410.0149).
- [44] Particle Data Group, C. Patrignani *et al.*, *Review of particle physics*, Chin. Phys. **C40** (2016) 100001.
- [45] T. Skwarnicki, *A study of the radiative cascade transitions between the Upsilon-prime and Upsilon resonances*, PhD thesis, Institute of Nuclear Physics, Krakow, 1986, DESY-F31-86-02.
- [46] K. S. Cranmer, *Kernel estimation in high-energy physics*, Comput. Phys. Commun. **136** (2001) 198, [arXiv:hep-ex/0011057](https://arxiv.org/abs/hep-ex/0011057).
- [47] LHCb collaboration, R. Aaij *et al.*, *Measurement of the track reconstruction efficiency at LHCb*, JINST **10** (2015) P02007, [arXiv:1408.1251](https://arxiv.org/abs/1408.1251).

- [48] M. Pivk and F. R. Le Diberder, *sPlot: A statistical tool to unfold data distributions*, Nucl. Instrum. Meth. **A555** (2005) 356, arXiv:physics/0402083.
- [49] H.-S. Shao *et al.*, *Yields and polarizations of prompt J/ψ and $\psi(2S)$ production in hadronic collisions*, JHEP **05** (2015) 103, arXiv:1411.3300.
- [50] M. Cacciari, M. Greco, and P. Nason, *The p_T spectrum in heavy-flavour hadroproduction*, JHEP **05** (1998) 007, arXiv:hep-ph/9803400.
- [51] P. Faccioli *et al.*, *Quarkonium production in the lhc era: A polarized perspective*, Physics Letters B **736** (2014) 98 .
- [52] M. Jacob and G. C. Wick, *On the general theory of collisions for particles with spin*, Annals Phys. **7** (1959) 404, Annals Phys. **281** (2000) 774.
- [53] LHCb collaboration, R. Aaij *et al.*, *Measurement of $\psi(2S)$ polarisation in pp collisions at $\sqrt{s} = 7$ TeV*, Eur. Phys. J. **C74** (2014) 2872, arXiv:1403.1339.
- [54] M. Cacciari, M. L. Mangano, and P. Nason, *Gluon PDF constraints from the ratio of forward heavy-quark production at the LHC at $\sqrt{S} = 7$ and 13 TeV*, Eur. Phys. J. **C75** (2015) 610, arXiv:1507.06197.

LHCb collaboration

R. Aaij³⁰, C. Abellán Beteta⁴⁷, B. Adeva⁴⁴, M. Adinolfi⁵¹, C.A. Aidala⁷⁷, Z. Ajaltouni⁸, S. Akar⁶², P. Albicocco²¹, J. Albrecht¹³, F. Alessio⁴⁵, M. Alexander⁵⁶, A. Alfonso Albero⁴³, G. Alkhazov³⁶, P. Alvarez Cartelle⁵⁸, A.A. Alves Jr⁴⁴, S. Amato², S. Amerio²⁶, Y. Amhis¹⁰, L. An²⁰, L. Anderlini²⁰, G. Andreassi⁴⁶, M. Andreotti¹⁹, J.E. Andrews⁶³, F. Archilli³⁰, J. Arnau Romeu⁹, A. Artamonov⁴², M. Artuso⁶⁴, K. Arzymatov⁴⁰, E. Aslanides⁹, M. Atzeni⁴⁷, B. Audurier²⁵, S. Bachmann¹⁵, J.J. Back⁵³, S. Baker⁵⁸, V. Balagura^{10,b}, W. Baldini¹⁹, A. Baranov⁴⁰, R.J. Barlow⁵⁹, S. Barsuk¹⁰, W. Barter⁵⁸, M. Bartolini²², F. Baryshnikov⁷³, V. Batozskaya³⁴, B. Batsukh⁶⁴, A. Battig¹³, V. Battista⁴⁶, A. Bay⁴⁶, J. Beddow⁵⁶, F. Bedeschi²⁷, I. Bediaga¹, A. Beiter⁶⁴, L.J. Bel³⁰, S. Belin²⁵, N. Belyi⁴, V. Bellee⁴⁶, N. Belloli^{23,i}, K. Belous⁴², I. Belyaev³⁷, G. Bencivenni²¹, E. Ben-Haim¹¹, S. Benson³⁰, S. Beranek¹², A. Berezhnoy³⁸, R. Bernet⁴⁷, D. Berninghoff¹⁵, E. Bertholet¹¹, A. Bertolin²⁶, C. Betancourt⁴⁷, F. Betti^{18,45}, M.O. Bettler⁵², Ia. Bezshyiko⁴⁷, S. Bhasin⁵¹, J. Bhom³², M.S. Bieker¹³, S. Bifani⁵⁰, P. Billoir¹¹, A. Birnkraut¹³, A. Bizzeti^{20,u}, M. Bjørn⁶⁰, M.P. Blago⁴⁵, T. Blake⁵³, F. Blanc⁴⁶, S. Blusk⁶⁴, D. Bobulska⁵⁶, V. Bocci²⁹, O. Boente Garcia⁴⁴, T. Boettcher⁶¹, A. Bondar^{41,w}, N. Bondar³⁶, S. Borghi^{59,45}, M. Borisjak⁴⁰, M. Borsato¹⁵, M. Boubdir¹², T.J.V. Bowcock⁵⁷, C. Bozzi^{19,45}, S. Braun¹⁵, M. Brodski⁴⁵, J. Brodzicka³², A. Brossa Gonzalo⁵³, D. Brundu^{25,45}, E. Buchanan⁵¹, A. Buonauro⁴⁷, C. Burr⁵⁹, A. Bursche²⁵, J. Buytaert⁴⁵, W. Byczynski⁴⁵, S. Cadeddu²⁵, H. Cai⁶⁸, R. Calabrese^{19,g}, R. Calladine⁵⁰, M. Calvi^{23,i}, M. Calvo Gomez^{43,m}, A. Camboni^{43,m}, P. Campana²¹, D.H. Campora Perez⁴⁵, L. Capriotti^{18,e}, A. Carbone^{18,e}, G. Carboni²⁸, R. Cardinale²², A. Cardini²⁵, P. Carniti^{23,i}, K. Carvalho Akiba², G. Casse⁵⁷, M. Cattaneo⁴⁵, G. Cavallero²², R. Cenci^{27,p}, M.G. Chapman⁵¹, M. Charles¹¹, Ph. Charpentier⁴⁵, G. Chatzikonstantinidis⁵⁰, M. Chefdeville⁷, V. Chekalina⁴⁰, C. Chen³, S. Chen²⁵, S.-G. Chitic⁴⁵, V. Chobanova⁴⁴, M. Chrzaszcz⁴⁵, A. Chubykin³⁶, P. Ciambrone²¹, X. Cid Vidal⁴⁴, G. Ciezarek⁴⁵, F. Cindolo¹⁸, P.E.L. Clarke⁵⁵, M. Clemencic⁴⁵, H.V. Cliff⁵², J. Closier⁴⁵, V. Coco⁴⁵, J.A.B. Coelho¹⁰, J. Cogan⁹, E. Cogneras⁸, L. Cojocariu³⁵, P. Collins⁴⁵, T. Colombo⁴⁵, A. Comerma-Montells¹⁵, A. Contu²⁵, G. Coombs⁴⁵, S. Coquereau⁴³, G. Corti⁴⁵, M. Corvo^{19,g}, C.M. Costa Sobral⁵³, B. Couturier⁴⁵, G.A. Cowan⁵⁵, D.C. Craik⁶¹, A. Crocombe⁵³, M. Cruz Torres¹, R. Currie⁵⁵, F. Da Cunha Marinho², C.L. Da Silva⁷⁸, E. Dall'Occo³⁰, J. Dalseno^{44,51}, C. D'Ambrosio⁴⁵, A. Danilina³⁷, P. d'Argent¹⁵, A. Davis⁵⁹, O. De Aguiar Francisco⁴⁵, K. De Bruyn⁴⁵, S. De Capua⁵⁹, M. De Cian⁴⁶, J.M. De Miranda¹, L. De Paula², M. De Serio^{17,d}, P. De Simone²¹, J.A. de Vries³⁰, C.T. Dean⁵⁶, W. Dean⁷⁷, D. Decamp⁷, L. Del Buono¹¹, B. Delaney⁵², H.-P. Dembinski¹⁴, M. Demmer¹³, A. Dendek³³, D. Derkach⁷⁴, O. Deschamps⁸, F. Desse¹⁰, F. Dettori⁵⁷, B. Dey⁶, A. Di Canto⁴⁵, P. Di Nezza²¹, S. Didenko⁷³, H. Dijkstra⁴⁵, F. Dordei²⁵, M. Dorigo^{45,x}, A.C. dos Reis¹, A. Dosil Suárez⁴⁴, L. Douglas⁵⁶, A. Dovbnya⁴⁸, K. Dreimanis⁵⁷, L. Dufour⁴⁵, G. Dujany¹¹, P. Durante⁴⁵, J.M. Durham⁷⁸, D. Dutta⁵⁹, R. Dzhelyadin^{42,†}, M. Dziewiecki¹⁵, A. Dziurda³², A. Dzyuba³⁶, S. Easo⁵⁴, U. Egede⁵⁸, V. Egorychev³⁷, S. Eidelman^{41,w}, S. Eisenhardt⁵⁵, U. Eitschberger¹³, R. Ekelhof¹³, L. Eklund⁵⁶, S. Ely⁶⁴, A. Ene³⁵, S. Escher¹², S. Esen³⁰, T. Evans⁶², A. Falabella¹⁸, C. Färber⁴⁵, N. Farley⁵⁰, S. Farry⁵⁷, D. Fazzini^{23,45,i}, M. Féo⁴⁵, P. Fernandez Declara⁴⁵, A. Fernandez Prieto⁴⁴, F. Ferrari^{18,e}, L. Ferreira Lopes⁴⁶, F. Ferreira Rodrigues², M. Ferro-Luzzi⁴⁵, S. Filippov³⁹, R.A. Fini¹⁷, M. Fiorini^{19,g}, M. Firlej³³, C. Fitzpatrick⁴⁶, T. Fiutowski³³, F. Fleuret^{10,b}, M. Fontana⁴⁵, F. Fontanelli^{22,h}, R. Forty⁴⁵, V. Franco Lima⁵⁷, M. Frank⁴⁵, C. Frei⁴⁵, J. Fu^{24,q}, W. Funk⁴⁵, E. Gabriel⁵⁵, A. Gallas Torreira⁴⁴, D. Galli^{18,e}, S. Gallorini²⁶, S. Gambetta⁵⁵, Y. Gan³, M. Gandelman², P. Gandini²⁴, Y. Gao³, L.M. Garcia Martin⁷⁶, J. García Pardiñas⁴⁷, B. Garcia Plana⁴⁴, J. Garra Tico⁵², L. Garrido⁴³, D. Gascon⁴³, C. Gaspar⁴⁵, G. Gazzoni⁸, D. Gerick¹⁵, E. Gersabeck⁵⁹, M. Gersabeck⁵⁹, T. Gershon⁵³, D. Gerstel⁹, Ph. Ghez⁷, V. Gibson⁵², O.G. Girard⁴⁶, P. Gironella Gironell⁴³, L. Giubega³⁵, K. Gizdov⁵⁵, V.V. Gligorov¹¹, C. Göbel⁶⁶, D. Golubkov³⁷, A. Golutvin^{58,73},

A. Gomes^{1,a}, I.V. Gorelov³⁸, C. Gotti^{23,i}, E. Govorkova³⁰, J.P. Grabowski¹⁵, R. Graciani Diaz⁴³, L.A. Granado Cardoso⁴⁵, E. Graugés⁴³, E. Graverini⁴⁷, G. Graziani²⁰, A. Grecu³⁵, R. Greim³⁰, P. Griffith²⁵, L. Grillo⁵⁹, L. Gruber⁴⁵, B.R. Gruberg Cazon⁶⁰, O. Grünberg⁷⁰, C. Gu³, E. Gushchin³⁹, A. Guth¹², Yu. Guz^{42,45}, T. Gys⁴⁵, T. Hadavizadeh⁶⁰, C. Hadjivasiliou⁸, G. Haefeli⁴⁶, C. Haen⁴⁵, S.C. Haines⁵², P.M. Hamilton⁶³, X. Han¹⁵, T.H. Hancock⁶⁰, S. Hansmann-Menzemer¹⁵, N. Harnew⁶⁰, T. Harrison⁵⁷, C. Hasse⁴⁵, M. Hatch⁴⁵, J. He⁴, M. Hecker⁵⁸, K. Heinicke¹³, A. Heister¹³, K. Hennessy⁵⁷, L. Henry⁷⁶, M. Heß⁷⁰, J. Heuel¹², A. Hicheur⁶⁵, R. Hidalgo Charman⁵⁹, D. Hill⁶⁰, M. Hilton⁵⁹, P.H. Hopchev⁴⁶, J. Hu¹⁵, W. Hu⁶, W. Huang⁴, Z.C. Huard⁶², W. Hulsbergen³⁰, T. Humair⁵⁸, M. Hushchyn⁷⁴, D. Hutchcroft⁵⁷, D. Hynds³⁰, P. Ibis¹³, M. Idzik³³, P. Ilten⁵⁰, A. Inglessi³⁶, A. Inyakin⁴², K. Ivshin³⁶, R. Jacobsson⁴⁵, S. Jakobsen⁴⁵, J. Jalocha⁶⁰, E. Jans³⁰, B.K. Jashal⁷⁶, A. Jawahery⁶³, F. Jiang³, M. John⁶⁰, D. Johnson⁴⁵, C.R. Jones⁵², C. Joram⁴⁵, B. Jost⁴⁵, N. Jurik⁶⁰, S. Kandybei⁴⁸, M. Karacson⁴⁵, J.M. Kariuki⁵¹, S. Karodia⁵⁶, N. Kazeev⁷⁴, M. Kecke¹⁵, F. Keizer⁵², M. Kelsey⁶⁴, M. Kenzie⁵², T. Ketel³¹, E. Khairullin⁴⁰, B. Khanji⁴⁵, C. Khurewathanakul⁴⁶, K.E. Kim⁶⁴, T. Kirn¹², V.S. Kirsebom⁴⁶, S. Klaver²¹, K. Klimaszewski³⁴, T. Klimkovich¹⁴, S. Koliiev⁴⁹, M. Kolpin¹⁵, R. Kopecna¹⁵, P. Koppenburg³⁰, I. Kostiuk^{30,49}, S. Kotriakhova³⁶, M. Kozeiha⁸, L. Kravchuk³⁹, M. Kreps⁵³, F. Kress⁵⁸, P. Krokovny^{41,w}, W. Krupa³³, W. Krzemien³⁴, W. Kucewicz^{32,l}, M. Kucharczyk³², V. Kudryavtsev^{41,w}, A.K. Kuonen⁴⁶, T. Kvaratskheliya^{37,45}, D. Lacarrere⁴⁵, G. Lafferty⁵⁹, A. Lai²⁵, D. Lancierini⁴⁷, G. Lanfranchi²¹, C. Langenbruch¹², T. Latham⁵³, C. Lazzeroni⁵⁰, R. Le Gac⁹, R. Lefèvre⁸, A. Leflat³⁸, F. Lemaitre⁴⁵, O. Leroy⁹, T. Lesiak³², B. Leverington¹⁵, P.-R. Li^{4,aa}, Y. Li⁵, Z. Li⁶⁴, X. Liang⁶⁴, T. Likhomanenko⁷², R. Lindner⁴⁵, F. Lionetto⁴⁷, V. Lisovskiy¹⁰, G. Liu⁶⁷, X. Liu³, D. Loh⁵³, A. Loi²⁵, I. Longstaff⁵⁶, J.H. Lopes², G. Loustau⁴⁷, G.H. Lovell⁵², D. Lucchesi^{26,o}, M. Lucio Martinez⁴⁴, Y. Luo³, A. Lupato²⁶, E. Luppi^{19,g}, O. Lupton⁴⁵, A. Lusiani²⁷, X. Lyu⁴, F. Machefert¹⁰, F. Maciuc³⁵, V. Macko⁴⁶, P. Mackowiak¹³, S. Maddrell-Mander⁵¹, O. Maev^{36,45}, K. Maguire⁵⁹, D. Maisuzenko³⁶, M.W. Majewski³³, S. Malde⁶⁰, B. Malecki⁴⁵, A. Malinin⁷², T. Maltsev^{41,w}, H. Malygina¹⁵, G. Manca^{25,f}, G. Mancinelli⁹, D. Marangotto^{24,q}, J. Maratas^{8,v}, J.F. Marchand⁷, U. Marconi¹⁸, C. Marin Benito¹⁰, M. Marinangeli⁴⁶, P. Marino⁴⁶, J. Marks¹⁵, P.J. Marshall⁵⁷, G. Martellotti²⁹, M. Martinelli⁴⁵, D. Martinez Santos⁴⁴, F. Martinez Vidal⁷⁶, A. Massafferri¹, M. Materok¹², R. Matev⁴⁵, A. Mathad⁵³, Z. Mathe⁴⁵, C. Matteuzzi²³, K.R. Mattioli⁷⁷, A. Mauri⁴⁷, E. Maurice^{10,b}, B. Maurin⁴⁶, M. McCann^{58,45}, A. McNab⁵⁹, R. McNulty¹⁶, J.V. Mead⁵⁷, B. Meadows⁶², C. Meaux⁹, N. Meinert⁷⁰, D. Melnychuk³⁴, M. Merk³⁰, A. Merli^{24,q}, E. Michielin²⁶, D.A. Milanes⁶⁹, E. Millard⁵³, M.-N. Minard⁷, O. Mineev³⁷, L. Minzoni^{19,g}, D.S. Mitzel¹⁵, A. Mödden¹³, A. Mogini¹¹, R.D. Moise⁵⁸, T. Mombächer¹³, I.A. Monroy⁶⁹, S. Monteil⁸, M. Morandin²⁶, G. Morello²¹, M.J. Morello^{27,t}, O. Morgunova⁷², J. Moron³³, A.B. Morris⁹, R. Mountain⁶⁴, F. Muheim⁵⁵, M. Mukherjee⁶, M. Mulder³⁰, D. Müller⁴⁵, J. Müller¹³, K. Müller⁴⁷, V. Müller¹³, C.H. Murphy⁶⁰, D. Murray⁵⁹, P. Naik⁵¹, T. Nakada⁴⁶, R. Nandakumar⁵⁴, A. Nandi⁶⁰, T. Nanut⁴⁶, I. Nasteva², M. Needham⁵⁵, N. Neri^{24,q}, S. Neubert¹⁵, N. Neufeld⁴⁵, R. Newcombe⁵⁸, T.D. Nguyen⁴⁶, C. Nguyen-Mau^{46,n}, S. Nieswand¹², R. Niet¹³, N. Nikitin³⁸, A. Nogay⁷², N.S. Nolte⁴⁵, A. Oblakowska-Mucha³³, V. Obraztsov⁴², S. Ogilvy⁵⁶, D.P. O'Hanlon¹⁸, R. Oldeman^{25,f}, C.J.G. Onderwater⁷¹, A. Ossowska³², J.M. Otalora Goicochea², T. Ovsiannikova³⁷, P. Owen⁴⁷, A. Oyanguren⁷⁶, P.R. Pais⁴⁶, T. Pajero^{27,t}, A. Palano¹⁷, M. Palutan²¹, G. Panshin⁷⁵, A. Papanestis⁵⁴, M. Pappagallo⁵⁵, L.L. Pappalardo^{19,g}, W. Parker⁶³, C. Parkes^{59,45}, G. Passaleva^{20,45}, A. Pastore¹⁷, M. Patel⁵⁸, C. Patrignani^{18,e}, A. Pearce⁴⁵, A. Pellegrino³⁰, G. Penso²⁹, M. Pepe Altarelli⁴⁵, S. Perazzini⁴⁵, D. Pereima³⁷, P. Perret⁸, L. Pescatore⁴⁶, K. Petridis⁵¹, A. Petrolini^{22,h}, A. Petrov⁷², S. Petrucci⁵⁵, M. Petruzzo^{24,q}, B. Pietrzyk⁷, G. Pietrzyk⁴⁶, M. Pikies³², M. Pili⁶⁰, D. Pinci²⁹, J. Pinzino⁴⁵, F. Pisani⁴⁵, A. Piucci¹⁵, V. Placinta³⁵, S. Playfer⁵⁵, J. Plews⁵⁰, M. Plo Casasus⁴⁴, F. Polci¹¹, M. Poli Lener²¹, A. Poluektov⁹, N. Polukhina^{73,c}, I. Polyakov⁶⁴, E. Polycarpo², G.J. Pomery⁵¹, S. Ponce⁴⁵, A. Popov⁴²,

D. Popov^{50,14}, S. Poslavskii⁴², E. Price⁵¹, J. Prisciandaro⁴⁴, C. Prouve⁴⁴, V. Pugatch⁴⁹,
 A. Puig Navarro⁴⁷, H. Pullen⁶⁰, G. Punzi^{27,p}, W. Qian⁴, J. Qin⁴, R. Quagliani¹¹, B. Quintana⁸,
 N.V. Raab¹⁶, B. Rachwal³³, J.H. Rademacker⁵¹, M. Rama²⁷, M. Ramos Pernas⁴⁴, M.S. Rangel²,
 F. Ratnikov^{40,74}, G. Raven³¹, M. Ravonel Salzgeber⁴⁵, M. Reboud⁷, F. Redi⁴⁶, S. Reichert¹³,
 F. Reiss¹¹, C. Remon Alepuz⁷⁶, Z. Ren³, V. Renaudin⁶⁰, S. Ricciardi⁵⁴, S. Richards⁵¹,
 K. Rinnert⁵⁷, P. Robbe¹⁰, A. Robert¹¹, A.B. Rodrigues⁴⁶, E. Rodrigues⁶²,
 J.A. Rodriguez Lopez⁶⁹, M. Roehrken⁴⁵, S. Roiser⁴⁵, A. Rollings⁶⁰, V. Romanovskiy⁴²,
 A. Romero Vidal⁴⁴, J.D. Roth⁷⁷, M. Rotondo²¹, M.S. Rudolph⁶⁴, T. Ruf⁴⁵, J. Ruiz Vidal⁷⁶,
 J.J. Saborido Silva⁴⁴, N. Sagidova³⁶, B. Saitta^{25,f}, V. Salustino Guimaraes⁶⁶, C. Sanchez Gras³⁰,
 C. Sanchez Mayordomo⁷⁶, B. Sanmartin Sedes⁴⁴, R. Santacesaria²⁹, C. Santamarina Rios⁴⁴,
 M. Santimaria^{21,45}, E. Santovetti^{28,j}, G. Sarpis⁵⁹, A. Sarti^{21,k}, C. Satriano^{29,s}, A. Satta²⁸,
 M. Saur⁴, D. Savrina^{37,38}, S. Schael¹², M. Schellenberg¹³, M. Schiller⁵⁶, H. Schindler⁴⁵,
 M. Schmelling¹⁴, T. Schmelzer¹³, B. Schmidt⁴⁵, O. Schneider⁴⁶, A. Schopper⁴⁵, H.F. Schreiner⁶²,
 M. Schubiger⁴⁶, S. Schulte⁴⁶, M.H. Schune¹⁰, R. Schwemmer⁴⁵, B. Sciascia²¹, A. Sciubba^{29,k},
 A. Semennikov³⁷, E.S. Sepulveda¹¹, A. Sergi⁵⁰, N. Serra⁴⁷, J. Serrano⁹, L. Sestini²⁶, A. Seuthe¹³,
 P. Seyfert⁴⁵, M. Shapkin⁴², T. Shears⁵⁷, L. Shekhtman^{41,w}, V. Shevchenko⁷², E. Shmanin⁷³,
 B.G. Siddi¹⁹, R. Silva Coutinho⁴⁷, L. Silva de Oliveira², G. Simi^{26,o}, S. Simone^{17,d}, I. Skiba¹⁹,
 N. Skidmore¹⁵, T. Skwarnicki⁶⁴, M.W. Slater⁵⁰, J.G. Smeaton⁵², E. Smith¹², I.T. Smith⁵⁵,
 M. Smith⁵⁸, M. Soares¹⁸, L. Soares Lavra¹, M.D. Sokoloff⁶², F.J.P. Soler⁵⁶, B. Souza De Paula²,
 B. Spaan¹³, E. Spadaro Norella^{24,q}, P. Spradlin⁵⁶, F. Stagni⁴⁵, M. Stahl¹⁵, S. Stahl⁴⁵,
 P. Steffko⁴⁶, S. Stefkova⁵⁸, O. Steinkamp⁴⁷, S. Stemmle¹⁵, O. Stenyakin⁴², M. Stepanova³⁶,
 H. Stevens¹³, A. Stocchi¹⁰, S. Stone⁶⁴, B. Storaci⁴⁷, S. Stracka²⁷, M.E. Stramaglia⁴⁶,
 M. Straticiuc³⁵, U. Straumann⁴⁷, S. Strokov⁷⁵, J. Sun³, L. Sun⁶⁸, Y. Sun⁶³, K. Swientek³³,
 A. Szabelski³⁴, T. Szumlak³³, M. Szymanski⁴, Z. Tang³, T. Tekampe¹³, G. Tellarini¹⁹,
 F. Teubert⁴⁵, E. Thomas⁴⁵, M.J. Tilley⁵⁸, V. Tisserand⁸, S. T'Jampens⁷, M. Tobin³³, S. Tolk⁴⁵,
 L. Tomassetti^{19,g}, D. Tonelli²⁷, D.Y. Tou¹¹, R. Tourinho Jadallah Aoude¹, E. Tournefier⁷,
 M. Traill⁵⁶, M.T. Tran⁴⁶, A. Trisovic⁵², A. Tsaregorodtsev⁹, G. Tuci^{27,p}, A. Tully⁵²,
 N. Tuning^{30,45}, A. Ukleja³⁴, A. Usachov¹⁰, A. Ustyuzhanin^{40,74}, U. Uwer¹⁵, A. Vagner⁷⁵,
 V. Vagnoni¹⁸, A. Valassi⁴⁵, S. Valat⁴⁵, G. Valenti¹⁸, M. van Beuzekom³⁰, E. van Herwijnen⁴⁵,
 J. van Tilburg³⁰, M. van Veghel³⁰, R. Vazquez Gomez⁴⁵, P. Vazquez Regueiro⁴⁴,
 C. Vázquez Sierra³⁰, S. Vecchi¹⁹, J.J. Velthuis⁵¹, M. Veltri^{20,r}, A. Venkateswaran⁶⁴, M. Vernet⁸,
 M. Veronesi³⁰, M. Vesterinen⁵³, J.V. Viana Barbosa⁴⁵, D. Vieira⁴, M. Vieites Diaz⁴⁴,
 H. Viemann⁷⁰, X. Vilasis-Cardona^{43,m}, A. Vitkovskiy³⁰, M. Vitti⁵², V. Volkov³⁸, A. Vollhardt⁴⁷,
 D. Vom Bruch¹¹, B. Voneki⁴⁵, A. Vorobyev³⁶, V. Vorobyev^{41,w}, N. Voropaev³⁶, R. Waldi⁷⁰,
 J. Walsh²⁷, J. Wang⁵, M. Wang³, Y. Wang⁶, Z. Wang⁴⁷, D.R. Ward⁵², H.M. Wark⁵⁷,
 N.K. Watson⁵⁰, D. Websdale⁵⁸, A. Weiden⁴⁷, C. Weisser⁶¹, M. Whitehead¹², G. Wilkinson⁶⁰,
 M. Wilkinson⁶⁴, I. Williams⁵², M. Williams⁶¹, M.R.J. Williams⁵⁹, T. Williams⁵⁰, F.F. Wilson⁵⁴,
 M. Winn¹⁰, W. Wislicki³⁴, M. Witek³², G. Wormser¹⁰, S.A. Wotton⁵², K. Wyllie⁴⁵, D. Xiao⁶,
 Y. Xie⁶, A. Xu³, M. Xu⁶, Q. Xu⁴, Z. Xu⁷, Z. Xu³, Z. Yang³, Z. Yang⁶³, Y. Yao⁶⁴,
 L.E. Yeomans⁵⁷, H. Yin⁶, J. Yu^{6,z}, X. Yuan⁶⁴, O. Yushchenko⁴², K.A. Zarebski⁵⁰,
 M. Zavertyaev^{14,c}, D. Zhang⁶, L. Zhang³, W.C. Zhang^{3,y}, Y. Zhang⁴⁵, A. Zhelezov¹⁵, Y. Zheng⁴,
 X. Zhu³, V. Zhukov^{12,38}, J.B. Zonneveld⁵⁵, S. Zucchelli^{18,e}.

¹Centro Brasileiro de Pesquisas Físicas (CBPF), Rio de Janeiro, Brazil

²Universidade Federal do Rio de Janeiro (UFRJ), Rio de Janeiro, Brazil

³Center for High Energy Physics, Tsinghua University, Beijing, China

⁴University of Chinese Academy of Sciences, Beijing, China

⁵Institute Of High Energy Physics (ihep), Beijing, China

⁶Institute of Particle Physics, Central China Normal University, Wuhan, Hubei, China

⁷Univ. Grenoble Alpes, Univ. Savoie Mont Blanc, CNRS, IN2P3-LAPP, Annecy, France

⁸Université Clermont Auvergne, CNRS/IN2P3, LPC, Clermont-Ferrand, France

- ⁹ Aix Marseille Univ, CNRS/IN2P3, CPPM, Marseille, France
¹⁰ LAL, Univ. Paris-Sud, CNRS/IN2P3, Université Paris-Saclay, Orsay, France
¹¹ LPNHE, Sorbonne Université, Paris Diderot Sorbonne Paris Cité, CNRS/IN2P3, Paris, France
¹² I. Physikalisches Institut, RWTH Aachen University, Aachen, Germany
¹³ Fakultät Physik, Technische Universität Dortmund, Dortmund, Germany
¹⁴ Max-Planck-Institut für Kernphysik (MPIK), Heidelberg, Germany
¹⁵ Physikalisches Institut, Ruprecht-Karls-Universität Heidelberg, Heidelberg, Germany
¹⁶ School of Physics, University College Dublin, Dublin, Ireland
¹⁷ INFN Sezione di Bari, Bari, Italy
¹⁸ INFN Sezione di Bologna, Bologna, Italy
¹⁹ INFN Sezione di Ferrara, Ferrara, Italy
²⁰ INFN Sezione di Firenze, Firenze, Italy
²¹ INFN Laboratori Nazionali di Frascati, Frascati, Italy
²² INFN Sezione di Genova, Genova, Italy
²³ INFN Sezione di Milano-Bicocca, Milano, Italy
²⁴ INFN Sezione di Milano, Milano, Italy
²⁵ INFN Sezione di Cagliari, Monserrato, Italy
²⁶ INFN Sezione di Padova, Padova, Italy
²⁷ INFN Sezione di Pisa, Pisa, Italy
²⁸ INFN Sezione di Roma Tor Vergata, Roma, Italy
²⁹ INFN Sezione di Roma La Sapienza, Roma, Italy
³⁰ Nikhef National Institute for Subatomic Physics, Amsterdam, Netherlands
³¹ Nikhef National Institute for Subatomic Physics and VU University Amsterdam, Amsterdam, Netherlands
³² Henryk Niewodniczanski Institute of Nuclear Physics Polish Academy of Sciences, Kraków, Poland
³³ AGH - University of Science and Technology, Faculty of Physics and Applied Computer Science, Kraków, Poland
³⁴ National Center for Nuclear Research (NCBJ), Warsaw, Poland
³⁵ Horia Hulubei National Institute of Physics and Nuclear Engineering, Bucharest-Magurele, Romania
³⁶ Petersburg Nuclear Physics Institute NRC Kurchatov Institute (PNPI NRC KI), Gatchina, Russia
³⁷ Institute of Theoretical and Experimental Physics NRC Kurchatov Institute (ITEP NRC KI), Moscow, Russia, Moscow, Russia
³⁸ Institute of Nuclear Physics, Moscow State University (SINP MSU), Moscow, Russia
³⁹ Institute for Nuclear Research of the Russian Academy of Sciences (INR RAS), Moscow, Russia
⁴⁰ Yandex School of Data Analysis, Moscow, Russia
⁴¹ Budker Institute of Nuclear Physics (SB RAS), Novosibirsk, Russia
⁴² Institute for High Energy Physics NRC Kurchatov Institute (IHEP NRC KI), Protvino, Russia, Protvino, Russia
⁴³ ICCUB, Universitat de Barcelona, Barcelona, Spain
⁴⁴ Instituto Galego de Física de Altas Enerxías (IGFAE), Universidade de Santiago de Compostela, Santiago de Compostela, Spain
⁴⁵ European Organization for Nuclear Research (CERN), Geneva, Switzerland
⁴⁶ Institute of Physics, Ecole Polytechnique Fédérale de Lausanne (EPFL), Lausanne, Switzerland
⁴⁷ Physik-Institut, Universität Zürich, Zürich, Switzerland
⁴⁸ NSC Kharkiv Institute of Physics and Technology (NSC KIPT), Kharkiv, Ukraine
⁴⁹ Institute for Nuclear Research of the National Academy of Sciences (KINR), Kyiv, Ukraine
⁵⁰ University of Birmingham, Birmingham, United Kingdom
⁵¹ H.H. Wills Physics Laboratory, University of Bristol, Bristol, United Kingdom
⁵² Cavendish Laboratory, University of Cambridge, Cambridge, United Kingdom
⁵³ Department of Physics, University of Warwick, Coventry, United Kingdom
⁵⁴ STFC Rutherford Appleton Laboratory, Didcot, United Kingdom
⁵⁵ School of Physics and Astronomy, University of Edinburgh, Edinburgh, United Kingdom
⁵⁶ School of Physics and Astronomy, University of Glasgow, Glasgow, United Kingdom
⁵⁷ Oliver Lodge Laboratory, University of Liverpool, Liverpool, United Kingdom
⁵⁸ Imperial College London, London, United Kingdom
⁵⁹ Department of Physics and Astronomy, University of Manchester, Manchester, United Kingdom

- ⁶⁰*Department of Physics, University of Oxford, Oxford, United Kingdom*
- ⁶¹*Massachusetts Institute of Technology, Cambridge, MA, United States*
- ⁶²*University of Cincinnati, Cincinnati, OH, United States*
- ⁶³*University of Maryland, College Park, MD, United States*
- ⁶⁴*Syracuse University, Syracuse, NY, United States*
- ⁶⁵*Laboratory of Mathematical and Subatomic Physics , Constantine, Algeria, associated to ²*
- ⁶⁶*Pontifícia Universidade Católica do Rio de Janeiro (PUC-Rio), Rio de Janeiro, Brazil, associated to ²*
- ⁶⁷*South China Normal University, Guangzhou, China, associated to ³*
- ⁶⁸*School of Physics and Technology, Wuhan University, Wuhan, China, associated to ³*
- ⁶⁹*Departamento de Fisica , Universidad Nacional de Colombia, Bogota, Colombia, associated to ¹¹*
- ⁷⁰*Institut für Physik, Universität Rostock, Rostock, Germany, associated to ¹⁵*
- ⁷¹*Van Swinderen Institute, University of Groningen, Groningen, Netherlands, associated to ³⁰*
- ⁷²*National Research Centre Kurchatov Institute, Moscow, Russia, associated to ³⁷*
- ⁷³*National University of Science and Technology “MISIS”, Moscow, Russia, associated to ³⁷*
- ⁷⁴*National Research University Higher School of Economics, Moscow, Russia, associated to ⁴⁰*
- ⁷⁵*National Research Tomsk Polytechnic University, Tomsk, Russia, associated to ³⁷*
- ⁷⁶*Instituto de Fisica Corpuscular, Centro Mixto Universidad de Valencia - CSIC, Valencia, Spain, associated to ⁴³*
- ⁷⁷*University of Michigan, Ann Arbor, United States, associated to ⁶⁴*
- ⁷⁸*Los Alamos National Laboratory (LANL), Los Alamos, United States, associated to ⁶⁴*
- ^a*Universidade Federal do Triângulo Mineiro (UFTM), Uberaba-MG, Brazil*
- ^b*Laboratoire Leprince-Ringuet, Palaiseau, France*
- ^c*P.N. Lebedev Physical Institute, Russian Academy of Science (LPI RAS), Moscow, Russia*
- ^d*Università di Bari, Bari, Italy*
- ^e*Università di Bologna, Bologna, Italy*
- ^f*Università di Cagliari, Cagliari, Italy*
- ^g*Università di Ferrara, Ferrara, Italy*
- ^h*Università di Genova, Genova, Italy*
- ⁱ*Università di Milano Bicocca, Milano, Italy*
- ^j*Università di Roma Tor Vergata, Roma, Italy*
- ^k*Università di Roma La Sapienza, Roma, Italy*
- ^l*AGH - University of Science and Technology, Faculty of Computer Science, Electronics and Telecommunications, Kraków, Poland*
- ^m*LIFAELS, La Salle, Universitat Ramon Llull, Barcelona, Spain*
- ⁿ*Hanoi University of Science, Hanoi, Vietnam*
- ^o*Università di Padova, Padova, Italy*
- ^p*Università di Pisa, Pisa, Italy*
- ^q*Università degli Studi di Milano, Milano, Italy*
- ^r*Università di Urbino, Urbino, Italy*
- ^s*Università della Basilicata, Potenza, Italy*
- ^t*Scuola Normale Superiore, Pisa, Italy*
- ^u*Università di Modena e Reggio Emilia, Modena, Italy*
- ^v*MSU - Iligan Institute of Technology (MSU-IIT), Iligan, Philippines*
- ^w*Novosibirsk State University, Novosibirsk, Russia*
- ^x*Sezione INFN di Trieste, Trieste, Italy*
- ^y*School of Physics and Information Technology, Shaanxi Normal University (SNNU), Xi'an, China*
- ^z*Physics and Micro Electronic College, Hunan University, Changsha City, China*
- ^{aa}*Lanzhou University, Lanzhou, China*

† Deceased